MICROWAVE COMPLEX PERMITTIVITIES OF AMORPHOUS AND ORGANIC SEMICONDUCTORS IN THE PRESENCE OF HIGH STEADY ELECTRIC FIELDS

A Thesis

Submitted to the

Faculty of Graduate Studies and Research

The University of Manitoba

In Partial Fulfillment

of the Requirements for the Degree of

Master of Science

by

Mohamed Atef Barakat

April, 1974

ABSTRACT

The microwave complex permittivities of the amorphous semiconductor $Si_{12}Ge_{10}As_{30}Te_{48}$ and anthracene organic crystals have been measured in the frequency range 1-4 GHz and 29-31 GHz in the presence of high steady electric fields, and at various temperatures. The results show that in amorphous semiconductors there is a resonance absorption at the frequency of 1.6 GHz, and the resonance frequency is strongly temperature dependent, and that in anthracene organic crystals the real part of the complex permittivity is independent of frequency in the frequency ranges from 1 to 4 GHz and from 29 to 31 GHz and not sensitive to temperature in the temperature range from 10 to 50°C. Within the frequency range under investigation the real part of the complex permittivity of both amorphous semiconductors and organic crystals is not affected by the applied steady electric field.

On the basis of the experimental results the resonance absorption phenomenon in the amorphous semiconductors is attributed to rotational vibration of dipoles, which may be formed by the aggregate of atoms of different types, about their equilibrium position. Because of low resonance frequency these dipoles are expected to be large in size and in moment of inertia. For anthracene organic crystals the real part of complex permittivity may be due mainly to electronic polarization.

ACKNOWLEDGEMENT

The author wishes to express his grateful appreciation to Professor K.C. Kao for suggesting this thesis subject and for his supervision through the entire work.

The author wishes also to express his sincere thanks to Professor E. Bridges and Dr. S.S. Stuchly for their valuable guidance and assistance in instrumentation and their deep interest in the project.

Sincere thanks are given to the graduate students of the Materials Research Laboratory and the staff of the Electrical Engineering Department of the University of Manitoba for their assistance and co-operation.

Finally, this research was supported by the National Research Council of Canada under grant number A3339, and the Defence Research Board of Canada under grant number 5566-39.

TABLE OF CONTENTS

PAGE

LIST OF FIGURES

FIGURE PAGE

LIST OF SYMBOLS

a	waveguide width
b	waveguide height
C	capacitance
C_o	capacitance of empty sample holder
e	electronic charge
E	electric field
E_o	average d.c. bias field
E_{ac}	microwave field
ε	carrier energy
ε_L	thermal equilibrium energy of carriers
f	distribution function of carriers
h	Planck's constant
$\hbar$	$h/2\pi$
J	current density
K_{nm}	wave number
K_o	free space wave number
K_E	component of wave vector in the field direction
K_B	Boltzmann constant
ℓ	sample length
m^*	effective mass of the electron
m_D	density of state mass
N	density of carriers
S	standing wave ratio
S_o	short circuit standing wave ratio
t	thickness of semiconductor slab
T	absolute temperature

T^*	complex transmission coefficient
V	displaced velocity in displaced Maxwellian distribution function
v_d	carrier drift velocity
Z_o	characteristic impedance
Z_c	impedance of capacitor sample holder
α	attenuation constant
γ^*	complex propagation constant
μ	electron mobility
σ	conductivity
$\sigma(\omega)$	small signal conductivity
σ_R	real part of conductivity
τ	relaxation time
τ_m	momentum relaxation time
τ_n	energy relaxation time
ε_r^*	complex relative permittivity
$\varepsilon_r(\omega)$	small signal relative permittivity (or dielectric constant)
ε'	real part of permittivity
ε''	imaginary part of permittivity
ε_∞	dielectric constant at infinite frequency
ϕ	phase shift
λ	wave length in free space
λ_g	guide wave length
ω	angular frequency
ω_o	resonance angular frequency
ξ	dipole moment

CHAPTER 1

INTRODUCTION

The study of high field transport phenomena in semiconductors has received much attention during the past two decades. The progress towards detailed understanding of high-field effects actually began in 1951 when the first high field experiments on Ge and Si were carried out by Shockley and Ryder [53, 57]. Since then, intensive efforts have been made to explore the high-field or the so-called hot electron transport phenomena in semiconductors.

The study of high-field transport is of considerable practical interest. Many solid state electronic devices are either based on some effects of high fields on the carriers or necessarily involve this in their operation.

The complex permittivity is one of the important parameters governing the properties of semiconductors. Thus, the study of this parameter under various conditions may lead to a better understanding of the structure of the materials and to some guidelines to their practical applications.

The present project is mainly concerned with the microwave complex permittivities of the amorphous semiconductor $Si_{12}\ Ge_{10}\ As_{30}\ Te_{48}$ and anthracene organic crystals in the presence of high steady electric fields. In the case of amorphous semiconductors, the present theory of solid state physics is apparently unable to explain the optical, electrical, and thermal properties of these materials, while in organic crystals the behaviour of Π-electrons is still not fully understood. $Si_{12}\ Ge_{10}\ As_{30}\ Te_{48}$ has been used as the model sample for the study

of amorphous semiconductors and anthracene as the model sample for that of organic crystals, This is one of the major reasons of choosing these materials for the present investigation. The behaviour of their complex permittivity as a function of frequency, temperature, and applied bias field has been studied in the hope that this would provide further insight into the properties of these materials.

Chapter 2 presents a brief review of previous theoretical and experimental work and Chapter 3 the experimental techniques and theory used to determine the complex permittivities from the measured parameters. The experimental procedures and microwave circuits used are described in detail in Chapter 4, the experimental results and discussion are given in Chapter 5, and conclusions arising from this investigation in Chapter 6.

CHAPTER 2

REVIEW OF PREVIOUS WORK

The earliest work on the effect of high electric fields on the behaviour of electrons in solids was carried out in connection with dielectric breakdown in insulators. Theoretical studies of the effect of high fields on the distribution function and mobility of electrons in semiconductors were first carried out in the 1930's [14, 15] but experimental results in this field were not available until 1951 [53, 57]. Shockley [57] and Ryder [53] were the first to show experimentally that at room temperature and 78°K the mobility of carriers in lightly doped germanium and silicon decreases with increasing field under high electric fields (higher than 1 KV/cm); they attributed this to an increase in energy of the carriers by the applied field. Shockley [57] has also calculated the carrier mobility for n-germanium as a function of field and his results are in agreement with the experiments.

Electric conductivities at high electric fields have been extensively studied in germanium and silicon of various types and concentrations of dopents and at various temperatures, in III-V compounds, and in other semiconductors. Large mobility changes with electric field have been found not to be due to change of electron energy, particularly in piezoelectric materials such as CdS and ZnO [12]. In well-doped CdS crystals, the current is ohmic up to the field for which the electron drift velocity approaches the sound velocity and tends to saturate or to increase slowly with increasing field [58]. The monohmic behaviour has been shown to arise from the generation of acoustic flux by the carriers, which takes place when the drift velocity exceeds the

sound velocity.

Application of a high field to a metal would not produce significant change in electron temperature, because the average electron energy is already high even without field. Hot electrons have, however, been introduced into a metal by tunneling from another metal or a semiconductor when appropriately biased [40, 59, 60]. In this situation the properties of greatest interest are the rate of energy loss and the mean free path of the electrons.

Not all of the conductivity changes observed in high fields are due to the change in mobility. Changes have been observed at low temperatures in germanium [1, 32, 54, 55], silicon [66], GaAs [45] due to impact ionization of shallow-level impurities by the hot carriers. In InSb, large changes at room temperatures and below have been shown to be due to impact ionization of the lattice by hot carriers [50, 61].

Theoretical approaches to high field transport phenomena are mainly based on the determination of the carrier distribution function for a given condition by solving the Boltzmann transport equation [36, 46]. In the following we briefly review some previous work in this field.

2.1. *Experimental Approaches*

One of the early experiments employing microwave techniques to study absorption properties of semiconductors subjected to a high dc field is that of Arther et al [4]. In their experiment, the semiconductor sample was cut in the form of a rectangular slab and inserted into the waveguide through a narrow slot cut in the center of the broad faces of the guide. The dc field was applied parallel to the microwave electric

field. They have found that microwave attenuation in n-Ge of 5 ohm-cm resistivity decreases with increasing applied dc field. Since the d.c. field is parallel to the microwave electric field and the latter is much smaller than the former, the field due to microwave radiation represents a small oscillation around the mean applied field and so the absorption is proportional to the differential mobility at that applied field. Figure 2.1 shows the electron velocity as a function of applied d.c. field with the saturation velocity at about 4.5 KV/cm, and this is in general agreement with that theoretically predicted by Ryder and Shockley [14, 15].

Using the same sample and waveguide geometry as those of Arther et al, Gibson et al [21], have measured the attenuation and phase shift of the sample holder at a frequency of 34.75 GHz under various d.c. fields, and found that the mobility at this microwave frequency is intermediate between the mobility (v/E) and differential mobility (dv/dE) obtained from the variation of carrier velocity with electric field. They have also found that the contribution of free carriers to the dielectric constant is negative at zero field but becomes positive at high fields. Their results for n-Ge is shown in Fig. 2.2 and Fig. 2.3. It is interesting to note that electron carriers in n-type materials follow these theoretical predictions, but not holes in p-type materials.

Another experiment was carried out by Zucker et al [71] involving the heating of charge carriers by large d.c. pulses and superimposing on these a small microwave electric field parallel to the d.c. field. In their experiment the sample was shaped in the form of a thin filament and then inserted into a small circular slot cut in the broad faces of a waveguide which was shorted one quarter of a guide-wavelength beyond

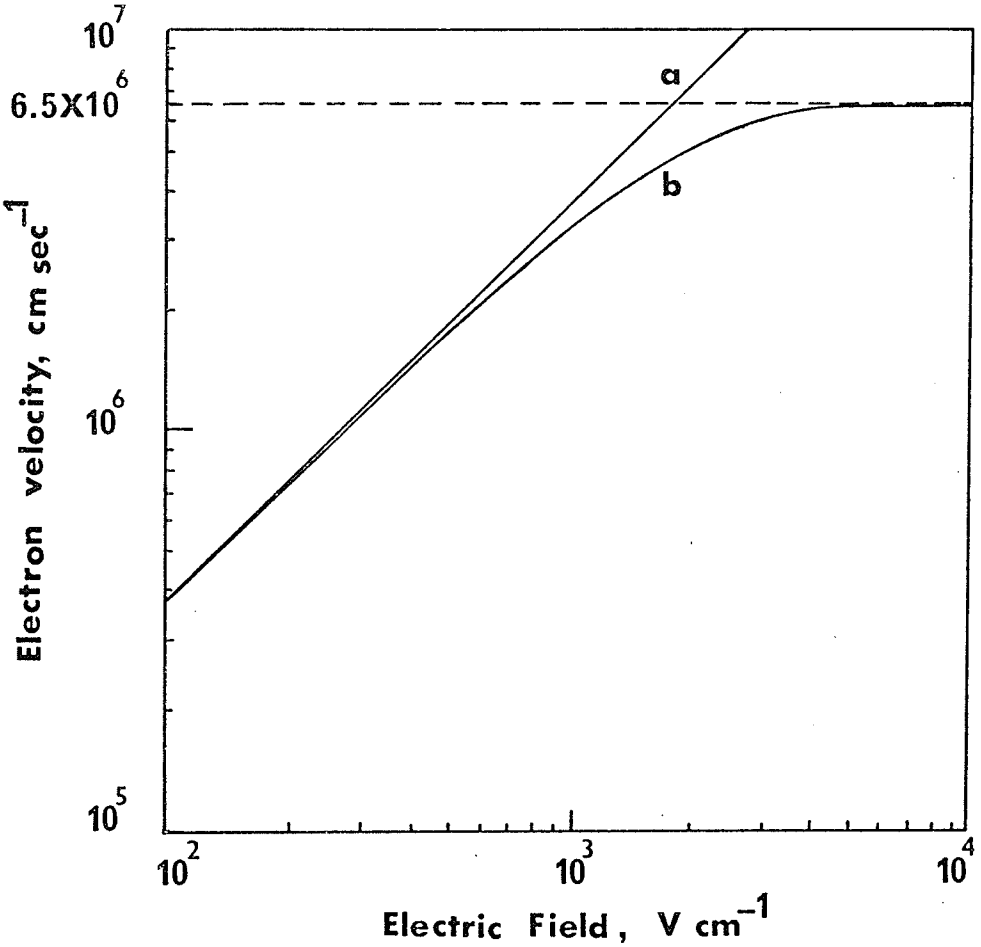

Fig. 2.1. Variation of electron velocity with electric field
a - Electron velocity in the ohmic region; b - Actual electron velocity at high fields for 5 ohm-cm n-Ge crystals (After Arther et al [4])

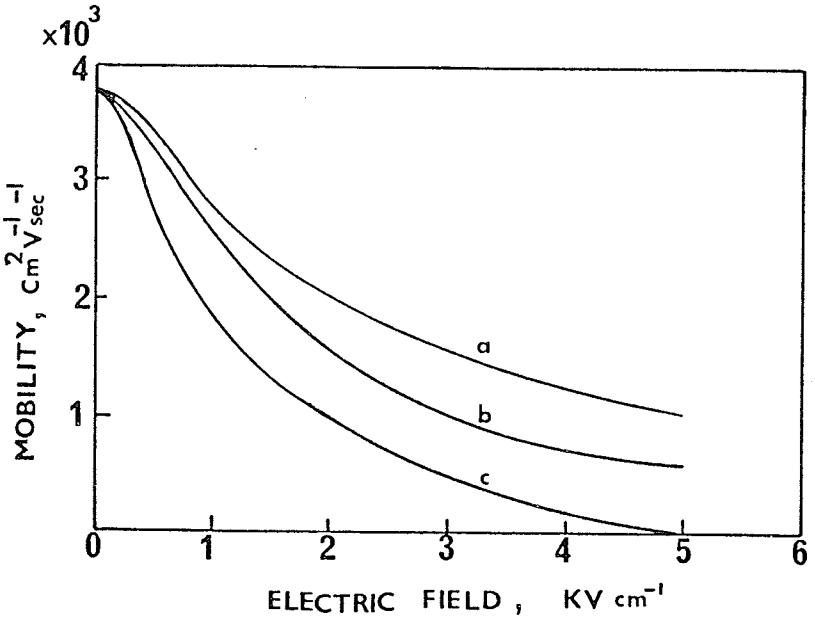

Fig. 2.2. Electron mobility as a function of d.c bias field E_{dc} for n-Ge of resistivity 4.7 ohm-cm, at 300°. a - d.c. mobility; b - small-signal 34.75 KMc/sec mobility; c = dv_d/dE. (After Gibson et al [21])

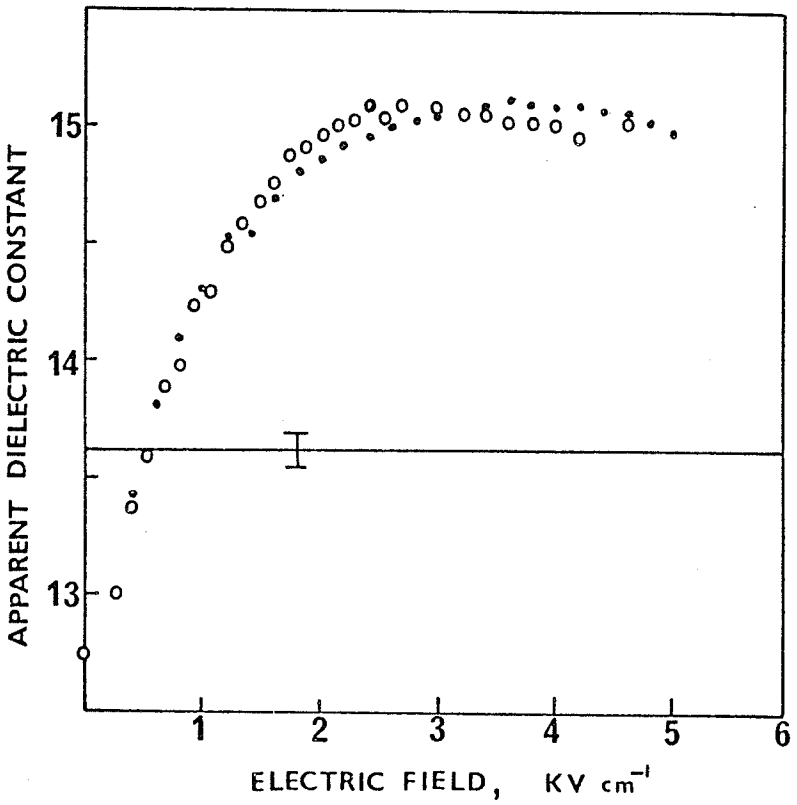

Fig. 2.3. Small-signal 34.75 KMc/sec dielectric constant as a function of dc bias field E_{dc} for the sample of Fig. 2.2. O-observed dielectric constant; - dielectric constant deduced from absorption data. (After Gibson et al [21])

the sample. The conductivity and dielectric constant as functions of applied d.c. field at a frequency of 70 GHz for moderately doped n-Ge samples are shown in Figs. 2.4 and 2.5. They have also reported that such a field dependent phenomenon of the conductivity and dielectric constant for n-Ge depends also on crystal orientation. The d.c. conductivity and small signal dielectric constant as functions of the d.c. bias fields, taken along differnt crystal orientations and at 77°K, are shown in Figs. 2.6 and 2.7. The effect of crystal anisotropy on conductivity is maximum at about 1KV/cm, and tends to decrease at higher fields. In general, the conductivity decreases monotomically with increasing fields while the small signal dielectric constant usually increases with electric field, reaches a maximum value at a specific value, and then decreases again with field. This phenomenon of anisotropy has also been observed in n-Si [27]. Using a method similar to that of Gibson et al, Gunn [24] showed by differentiating graphically the d.c. mobility curve that the a.c. mobility equals the differential mobility. A similar phenomenon has also been observed in n-InSb [12] and some results are shown in Figs. 2.8 and 2.9. The sharp rise in conductivity and decrease in dielectric constant occurring at higher fields are attributed to the increase in carrier concentration due to impact ionization [12].

The effect of d.c. bias field on microwave complex permittivity of n-Si and n-GaAs at various temperatures has been studied by Wu et al [68], using the frequency 9.03 KMc/sec and applied d.c. field up to 4.5 KV/cm. Their results are shown in Figs. 2.10 and 2.11. Glover [22] has also measured relative permittivity and microwave conductivity of n-GaAs at 35 GHz as functions of applied d.c. field up to fields of

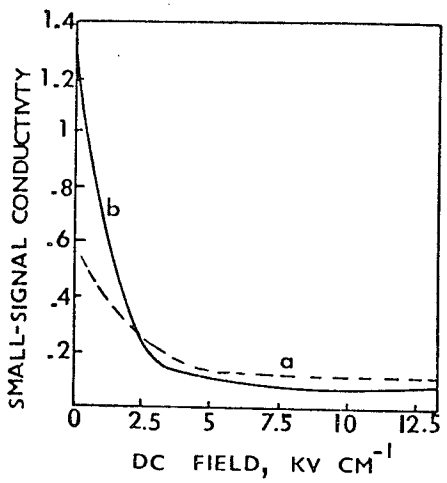

Fig. 2.4. Small-signal 70 KMc/sec conductivity as a function of bias field for n-Ge of low field sensitivity of 1.9 ohm-cm (at 300°K). Temperature a, 300°K; b, 78°K, (After Zucker et al [71].

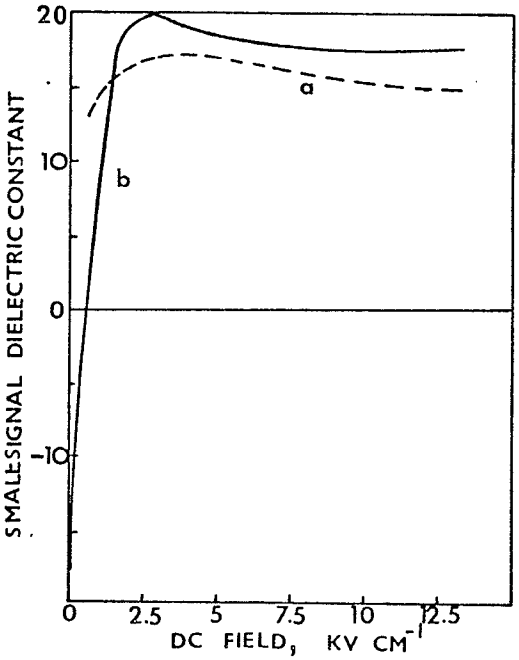

Fig. 2.5. Small-signal 70 KMc/sec dielectric constant as a function of d.c. bias field for the sample of Fig. 2.4. Temperature: a, 300°K; b, 78°K. (After Zucker et al [71]).

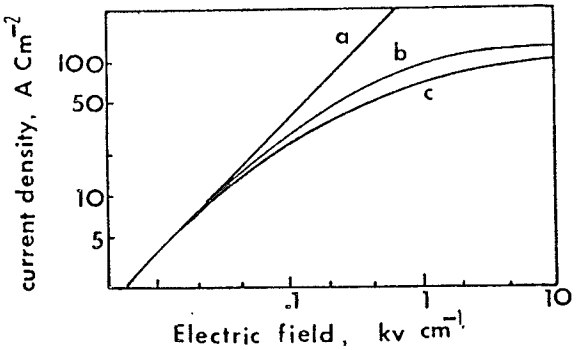

Fig. 2.6. Current density as a function of d.c. bias electric field at 77°K for two orientations of n-Ge of resistivity 18 ohm-cm (at 300°K). a - calcualted curve for the <110> orientation; b - measured curve for <110>; c - <111> . (After Nathan [44]).

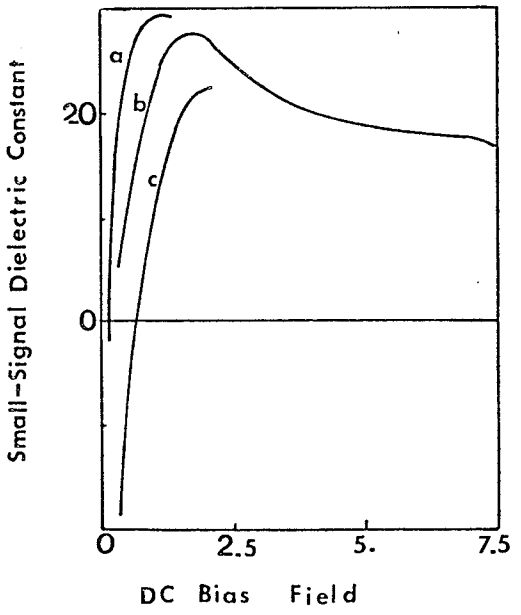

Fig. 2.7. Small-signal 70 GHz dielectric constant as a function of bias field at 78°K for n-Ge of room temperature resistivity of 1 to 2 ohm-cm for different orientation. Orientation: a, <100>; b, <110>; c, <111> . (After Conwell [12]).

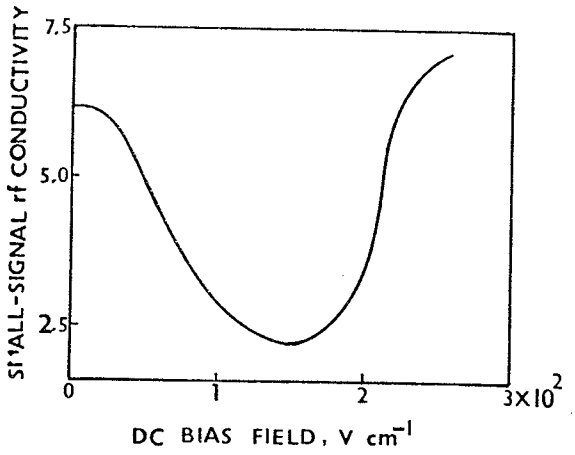

Fig. 2.8. Small-signal 69.25 KMc/sec conductivity as a function of d.c. bias field for n-InSb of low-field resistivity of 0.1 ohm-cm at 78°K. (After Conwell [12]).

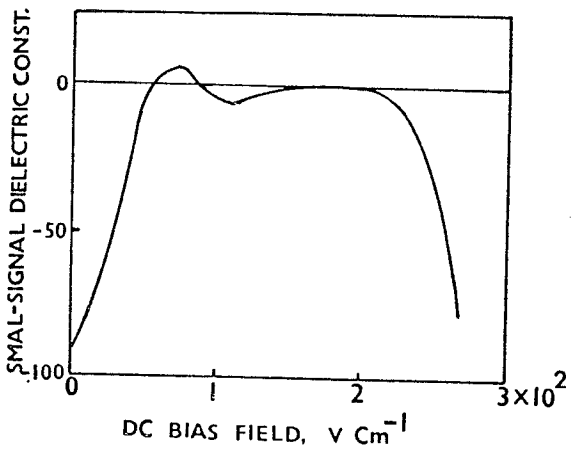

Fig. 2.9. Small-signal 69.25 KMc/sec dielectric constant as a function of d.c. bias field for the InSb sample of Fig. 2.8. (After Conwell et al [12]).

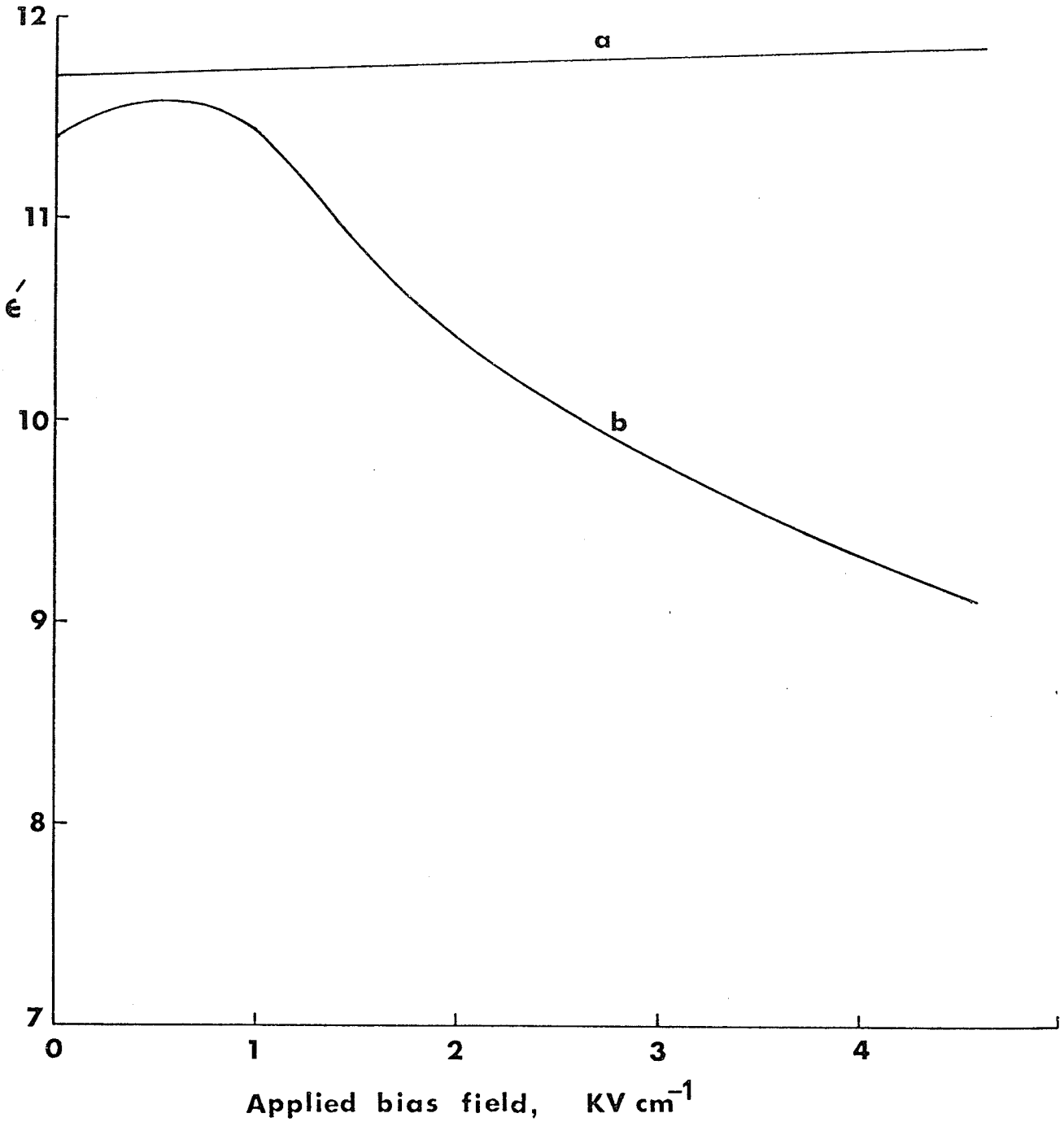

Fig. 2.10. Relative real permittivity ε' of silicon as a function of d.c. bias field. Temperature: a, 300°K; b, 95°K. (After Wu et al [68]).

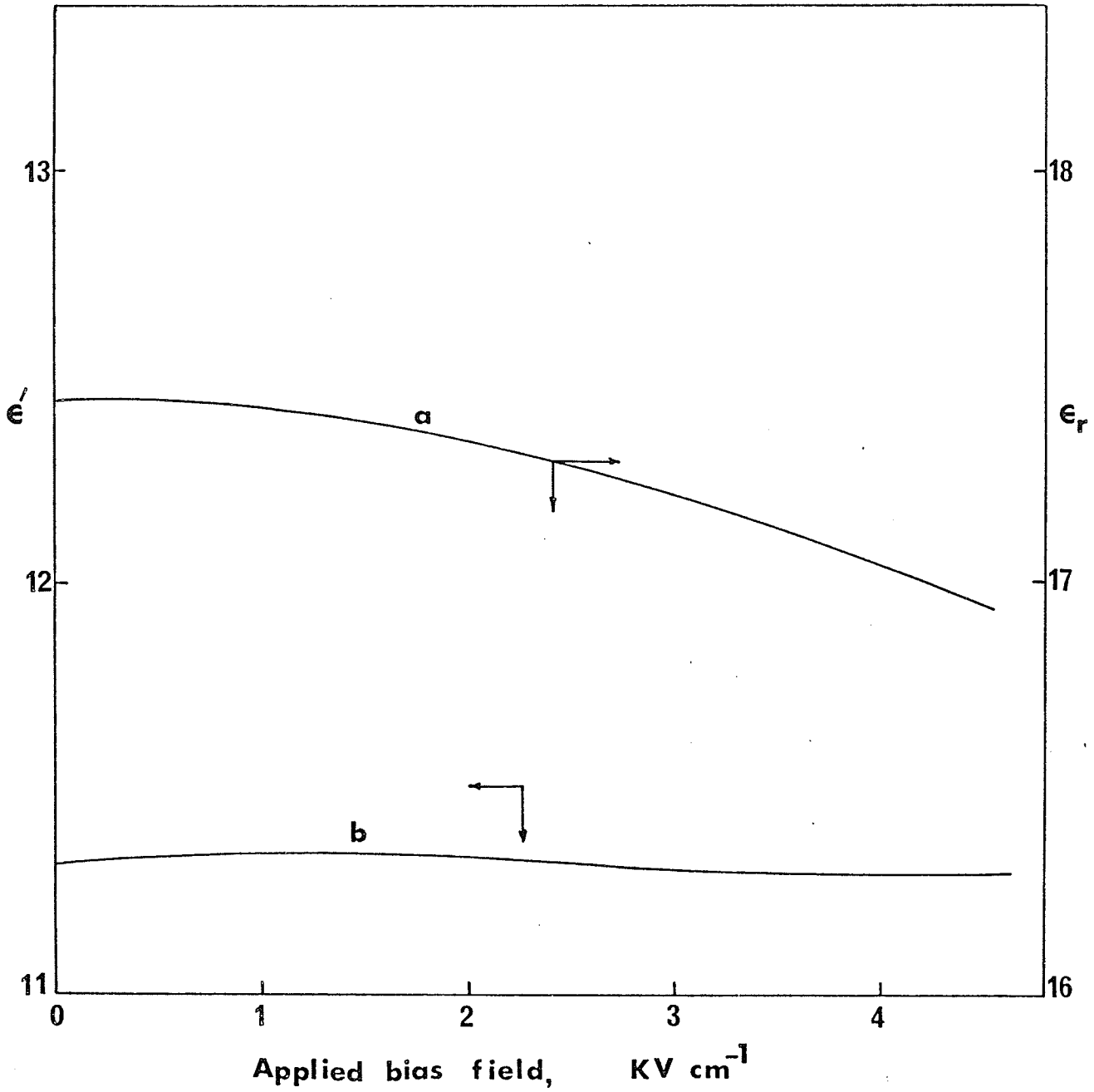

Fig. 2.11. Relative real permittivity ε' of n-GaAs as a function of d.c. bias field. Temperature: a, 95°K; b, 300°K. Resistivity a, 1.72 ohm-cm; b, 23 ohm-cm. (After Wu et al [68]).

16 KV/cm and his results are shown in Figs. 2.12 and 2.13. The large-signal and small-signal permittivities of n-GaAs converge only at low-fields where electron inertia due to momentum relaxation is the only process of importance. At higher fields, thermal relaxation processes predominate with different effects in the two cases. The small-signal permittivity shows a large sharply peaked maximum at a field near the threshold value. The large-signal permittivity, on the other hand, has a comparatively much smaller and broader peak occuring at a field higher than the threshold. The large signal permittivity is defined as an average over large signal swings.

2.2. *Theoretical Approaches*

The d.c. bias dependence of the microwave complex permittivity can be analysed on the basis of conservation of energy and momentum [21]. This approach can further be simplified if a δ function distribution can be used to represent the distribution of all carriers having the same energy, and the constant energy surfaces can be assumed to be spherical.

The rate of change of net momentum of carriers in an electric field is given by

$$\frac{d(m^*\bar{v}_d)}{dt} = e\,\bar{E} - \frac{m^*\bar{v}_d}{\tau_m} \qquad (2.1)$$

where the first term represents the rate of gain of momentum from the field and the second term represents the rate of loss of momentum to the lattice, τ_m being the momentum relaxation time.

The average rate of change of carrier energy in the field is

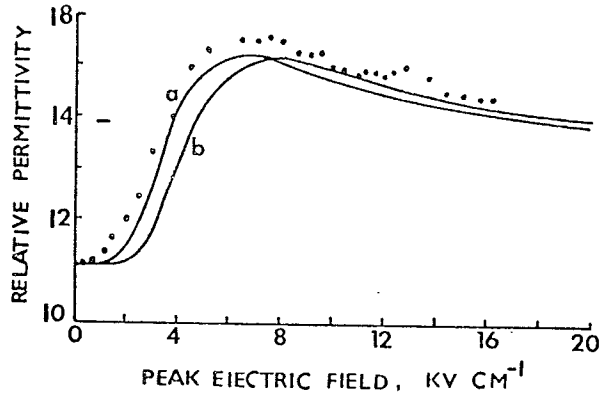

Fig. 2.12. Measured (data points) and calculated relative permittivity as functions of peak microwave field for n-GaAs at 35 GHz. (After Glover [22]).

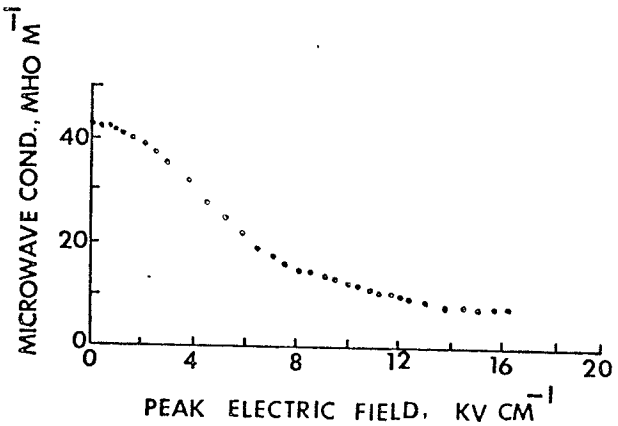

Fig. 2.13. Measured microwave conductivity as a function of peak microwave field for n-GaAs at 35 GHz (After Glover [22]).

$$\frac{d\varepsilon}{dt} = e\,\bar{v}_d \cdot \bar{E} - \frac{\varepsilon - \varepsilon_L}{\tau_\varepsilon} \tag{2.2}$$

where the rate of loss of energy to the lattice, represented by the second term on the right, has been assumed to be proportional to the excess of energy over the thermal equilibrium value ε_L. The quantity τ_ε is the energy relaxation time which in general is a function of carrier energy.

In the presence of a high d.c. field, but in the absence of any microwave field, Eq. (2.2) in steady state becomes

$$\begin{aligned} \varepsilon_o - \varepsilon_L &= e\,\tau_{\varepsilon o}\, v_{do}\, \bar{E}_o \\ &= \left(\frac{e^2}{m^*}\right) \tau_{\varepsilon o}\, \tau_{mo}\, \bar{E}_o^2 \end{aligned} \tag{2.3}$$

where the subscript "0" indicates d.c. equilibrium conditions. When a small microwave electric field is superimposed in a direction parallel to the d.c. field $\bar{E}_o$, the total energy and drift velocity of the carriers can be written as

$$\begin{aligned} \varepsilon &= \varepsilon_o + \Delta\varepsilon \\ \bar{v}_d &= \bar{v}_{do} + \Delta\bar{v}_d \end{aligned} \tag{2.4}$$

in which $\Delta\varepsilon << \varepsilon_o$ and $\Delta\bar{v}_d << \bar{v}_{do}$. By assuming that the energy dependence of τ_m and τ_ε can be written in the form

$$\begin{aligned} \tau_m &= a\,\varepsilon^{-n_1}, \\ \tau_\varepsilon &= b\,\varepsilon^{-n_2} \end{aligned} \tag{2.5}$$

where n_1 and n_2 are constants. Then in the presence of a small microwave field τ_m and τ_ε can be well approximated by

$$\tau_m^{-1} = \tau_{mo}^{-1}(1 + n_1 \frac{\Delta\varepsilon}{\varepsilon_o}) \ ,$$
$$\tau_\varepsilon^{-1} = \tau_{\varepsilon o}^{-1}(1 + n_2 \frac{\Delta\varepsilon}{\varepsilon_o}) \qquad (2.6)$$

Writing the microwave field as $E_{ac}\, e^{i\omega t}$ and substituting Eqs. (2.4) and (2.5) into Eqs. (2.1) and (2.2), we obtain the first order approximation.

$$\frac{d\Delta v_d}{dt} = \frac{e\, E_{ac}\, e^{i\omega t}}{m^*} - \frac{\Delta v_d}{\tau_{mo}} - n_1 \frac{v_{do}}{\tau_{mo}} \frac{\Delta\varepsilon}{\varepsilon_o} \qquad (2.7)$$

or

$$\frac{d\Delta\varepsilon}{dt} = e\, v_{do}\, E_{ac}\, e^{i\omega t} + e\, \Delta v_d\, E_o - \frac{\Delta\varepsilon}{\varepsilon_o}\left[1 + n_2\left(\frac{\varepsilon_o - \varepsilon_L}{\varepsilon_o}\right)\right] \qquad (2.8)$$

The first two terms on the right-hand side of Eq. (2.7) give the complete effect of the microwave field on momentum when the energy of the carriers remains unchanged. The third term shows the change in τ_m with energy. The first two terms on the right-hand side of Eq. (2.8) represent the first order change in the rate of energy gain due to the superposition of the microwave field on the d.c. field, whereas the third term gives the change in the rate of energy flow because of the changes in ε and τ_ε.

The complex conductivity $\sigma(\omega)$, related to Δv_d, is given by

$$\sigma(\omega) = \frac{ne\, \Delta v_d}{E_{ac}\, e^{i\omega t}} \qquad (2.9)$$

By making the approximations,

$$(\omega \tau_m)^2 << 1 \ , \text{ and}$$
$$\tau_\varepsilon >> \tau_m \ , \qquad (2.10)$$

are reasonable for the frequencies and materials used in the previously cited investigations, though the second

condition in Eq. (2.10) (i.e. $\tau_\varepsilon >> \tau_m$) is not well satisfied for carriers with energies greater than the optical phonon energy; the real part of the conductivity can be expressed as

$$\sigma_R = \sigma_o\left(1 - \frac{\Omega\Pi}{1 + \omega^2\Pi^2}\right) \tag{2.11}$$

where σ_o is the conductivity at the field $\bar{E}_o$, and

$$\Omega = 2n_1(\varepsilon_o - \varepsilon_L)/\tau_{\varepsilon o}\,\varepsilon_o \tag{2.12}$$

and

$$\Pi = \tau_{\varepsilon o}[1 + (n_1 + n_2)(\varepsilon_o - \varepsilon_L)/\varepsilon_o]^{-1} \ . \tag{2.13}$$

Using the imaginary part of the conductivity and Eq. (2.6), the high frequency dielectric constant can be written as

$$\varepsilon_r(\omega) = \varepsilon_{r(lat)} - 4\pi\frac{\sigma_o}{\varepsilon_o}\left(\tau_{mo} - \frac{\Omega\Pi^2}{1 + \omega^2\Pi^2}\right) \ . \tag{2.14}$$

It can be seen from Eqs. (2.11) - (2.14) that if τ_m is independent of carrier energy, or if n_1 is zero; σ_R and $\varepsilon_r(\omega)$ would have values appropriate to those at a d.c. field $\bar{E}_o$. The in-phase modulation of τ_m gives rise to the second term of Eq. (2.11), whereas the out-of-phase term tends to counteract the usual contribution of carriers to $\varepsilon_r(\omega)$ provided that $n_1 > o$. This is the origin of the increase in $\varepsilon_r(\omega)$ found experimentally at high bias fields.

Arther et al [4] have reported that at low frequencies

$$\sigma = n\,e\,\frac{d\bar{v}_d}{d\bar{E}} \tag{2.15}$$

From Eq. (2.11), for $\omega\Pi << 1$ and by setting $\sigma_R = ne\,\mu_{ac} = ne\left(\frac{d\bar{v}_d}{d\bar{E}}\right)$ we obtain

$$(1 - \Omega\Pi) = (1/\mu_{dc})\left(\frac{d\bar{v}_d}{d\bar{E}}\right) , \tag{2.16}$$

where μ_{dc} is the carrier mobility in the field $\bar{E}_o$. Thus from Eq. (2.11) we have

$$\Pi = \frac{1}{\omega}\left[\frac{\mu_{ac} - \frac{d\bar{v}_d}{d\bar{E}}}{\mu_{dc} - \mu_{ac}}\right]^{\frac{1}{2}} , \tag{2.17}$$

where all quantities on the right-hand side are directly measurable. Using this equation, Gibson et al [21] have found that the values of Π for n-Ge are in the range of 1 to 3×10^{-11} sec in the field range of 500-5000 V/cm. Once Π has been determined experimentally Eq. (2.11) and the measured σ_R and σ_o can be used to determine Ω. Since τ_{mo} can be deduced from d.c. data, all the quantities required to calculate $\varepsilon_r(\omega)$ can then be determined. However, the values of $\varepsilon_r(\omega)$ were calculated from Eq. (2.14) are in good agreement with experimental results for n-Ge but show poor argument for P-Ge.

To modify this theory, Gibson et al [21] have made the assumption that the carriers follow a drifted Maxwell-Boltzmann distribution and that the dominant scattering mechanisms are acoustic and optical phonon scattering; and obtain the momentum and energy balanced equations:

$$N\, m^* \frac{d\bar{v}_d}{dt} = Ne\,\bar{E} - \int_0^\infty \bar{V}\left[\left(\frac{\partial f}{\partial t}\right)_{aco} + \left(\frac{\partial f}{\partial t}\right)_{op}\right] d^3\bar{v} \tag{2.18}$$

$$N \frac{d\left(\frac{3}{2} K_B T\right)}{dt} = Ne\,\bar{v}_d \cdot \bar{E} - \int_0^\infty \varepsilon\left[\left(\frac{\partial f}{\partial t}\right)_{aco} + \left(\frac{\partial f}{\partial t}\right)_{op}\right] d^3\bar{v} \tag{2.19}$$

where $\left(\frac{\partial f}{\partial t}\right)_{aco}$ and $\left(\frac{\partial f}{\partial t}\right)_{op}$ are, respectively, the rates of change of the distribution function of the carriers due to scattering by acoustical and optical phonons; N and V are, respectively, the concentration and velocity of carriers; K_B and T are, respectively, the Boltzmann

constant and the temperature of carriers; and $\frac{3}{2} K_B T$ is the mean energy of the carriers; $\bar{v}_d$ is the displaced velocity as defined in the assumed drifted Maxwellian distribution function.

$$f(\bar{V}, \bar{v}_d, T) = N\left(\frac{m_D}{2\pi K_B T}\right)^{3/2} \exp\left(\frac{-m^* |\bar{V} - \bar{v}_d|}{2K_B T}\right) \tag{2.20}$$

in which m_D is the density of state mass. By neglecting terms of second and higher order of $\bar{v}_d$, we can write the distribution function in the form

$$f(\bar{V}, \bar{v}_d, T) = f_o + f_e \cos\theta \tag{2.21}$$

where

$$f_o(\varepsilon, T) = N\left(\frac{m_D}{2\pi K_B T}\right)^{3/2} \exp\left(-\frac{\varepsilon}{K_B T}\right) \tag{2.22}$$

$$f_e(\varepsilon, \bar{v}_d, T) = \frac{m^*}{K_B T} f_o |\bar{V}| |\bar{v}_d| \tag{2.23}$$

$$\cos\theta = \frac{\bar{V} \cdot \bar{E}}{|\bar{E}| |\bar{V}|} \tag{2.24}$$

Stratton [63] has obtained expressions for $\left(\frac{\partial f_o}{\partial t}\right)_{aco}$, $\left(\frac{\partial f_e}{\partial t}\right)_{aco}$, $\left(\frac{\partial f_o}{\partial t}\right)_{op}$ and $\left(\frac{\partial f_e}{\partial t}\right)_{op}$. Thus by substituting these expressions, in appropriate form, into Eqs. (2.18) and (2.19) a small signal analysis leads to first order expressions for $m^* \frac{d\,\Delta v_d}{dt}$ and $3/2\, K_B \frac{d\Delta T}{dt}$ in ΔV and ΔT. There expressions are similar to Eqs. (2.18) and (2.19) in form and therefore the solution for $\sigma(\omega)$ can be easily obtained. However, expressions for $\sigma(\omega)$ and $\varepsilon(\omega)$ and Π are the same as those given by Eqs. (2.11), (2.14), and (2.17), although Ω and Π are defined differently. In this theory Π is a sensitive function of the ratio of optical to acoustic mode coupling constants. Gibson et al have evaluated Π for n-Ge for different values of this ratio, ranging from

the value required to account for the temperature dependence of the mobility to values considerably lower. The experimental values obtained agree as to the order of magnitude of the theoretical value of Π over the range of bias fields from 0 to 5 KV/cm. However, Gibson et al were not able to duplicate the variation of Π with E for all values of the ratio of coupling constant and suggested that the most probable reason for the lack of agreement between theory and experiment is that at fields as low as 2 KV/cm, or higher, regions of momentum space are populated with carriers whose average effective mass is dependent upon their energy either through the departure from the parabolic relationship of ε and K with the <111> valleys, or through the population at $K = o$ minimum. Conwell [12], on the other hand, disagrees with this suggestion, because there is no evidence for a departure from the parabolic ε-K relation or a variation in effective mass, at fields as low as 2 KV/cm. Scattering to the $K=o$ minimum is not, in any case, expected to have much effect because of the small density of states in this minimum. However, the discrepancy between theory and experiment may also possibly be due to the use of the shifted Maxwell-Boltzmann distribution. This distribution would be particularly poor in the warm electron region, i.e., in fields up to about 2000V/cm. Another possible source of discrepancy between theory and experiment is the neglect of the relaxation due to intervalley scattering [34]. The intervalley scattering time has been shown to be of the order of the value τ_ε at 78°K. A simple treatment of the frequency dependence of the conductivity including relaxation repopulation as well as energy relaxation has been carried out by Schmidt-Tiedmann [56].

Using the same approach as that adopted by Gibson et al, Köpetz

and Pötzt [34] have analyzed the microwave conductivity under hot electron conditions.

The only theoretical approach to the problem of high field transport which has yielded quantitative results is through the solution of the Boltzmann equation [35, 36, 38]. The validity of the Boltzmann equation in the region of high fields has been partially investigated by Hasegawa and Yamashita [28]. Using a method similar to that of Kohn and Luttinger [33] for low fields, they have shown that for the simple band structure model, and for acoustic mode scattering only, the transport equation obtained from the equation of motion of the density matrix is equivalent to the Boltzmann equation. For their model, the solution of the Boltzmann equation may be expressed by a series of Legendre polynomials [13]

$$f(\varepsilon,x) = \sum_{n=o}^{\infty} G_n(\varepsilon)\, P_n(x) \tag{2.23}$$

where x is the cosine of the angle between $\bar{K}$ and $\bar{E}$. If the loss of carrier energy in a collision is only a small fraction of the total carrier energy and the scattering is not predominantly forward or backward, the distribution can be considered to be spherically symmetric [10]. In such a case all terms in the expansion in comparison with that for $n = o$ are small and in addition, it has been shown in most cases that $G_2(\varepsilon) << G_1(\varepsilon)$, and that $G_n(\varepsilon)$ for $n \geq 3$ are much smaller. Therefore, for the simple model and approximately elastic and isotropic scattering, a good approximation to the distribution function is obtained with only two terms in Eq. (2.23). Thus, we have

$$f = f_o(\varepsilon) + K_E\, g_e(\varepsilon) \tag{2.24}$$

where K_E is the component of $\bar{K}$ in the field direction. The Boltzmann equation is given by

$$\frac{\partial f}{\partial t} = \left(\frac{\partial f}{\partial t}\right)_E + \left(\frac{\partial f}{\partial t}\right)_c \tag{2.25}$$

where $\left(\frac{\partial f}{\partial t}\right)_E$ is the rate of change of the distribution function due to the field and it may be written as

$$\left(\frac{\partial f}{\partial t}\right)_E = -\frac{e\bar{E}}{\hbar} \cdot \nabla_K f$$

$$= -\frac{e\bar{E}}{\hbar}\left(g_e + \frac{2}{3}\,\varepsilon\, g_e' + \frac{\hbar^2 K_E}{m^*} f_o'\right) \tag{2.26}$$

For spherical constant energy surfaces and constant effective mass m^*; where the term $\frac{\hbar^2 K_E^2}{m^*}$ has been replaced by its average $\frac{2}{3}\varepsilon$; the prime represents differentiation with respect to ε; and $\left(\frac{\partial f}{\partial t}\right)_c$ is the rate of change of f due to scattering which is given by

$$\left[\frac{\partial (K_E\, g_e)}{\partial\, t}\right]_c = -\frac{K_e E\, g_e}{\tau} \tag{2.27}$$

where τ is the relaxation time due to elastic and randomising scattering processes. Thus, we can write the Boltzmann equation in the form

$$\left(\frac{\partial f_o}{\partial t}\right) - \frac{K_E\, g_e}{\tau} - \frac{eE}{\hbar}\left(g_e + \frac{2}{3}\, g_e' + \frac{h^2 K_E}{m^*}\, f_o'\right) = \frac{\partial f}{\partial t} \tag{2.28}$$

In the steady state, $\frac{\partial f}{\partial t} = o$, the coefficient of each Legendre polynomial vanishes, giving

$$\left(\frac{\partial f_o}{\partial t}\right)_c = \frac{eE}{\hbar}\left(g_e + \frac{2}{3}\,\varepsilon\, g_e'\right) \tag{2.29}$$

$$g_e = -\frac{h\, eE\, \tau}{m^*} f_o' \tag{2.30}$$

In the presence of a microwave field, Eq. (2.28) can take on the following forms

$$\left(\frac{\partial f_o}{\partial t}\right)_c - \frac{2}{3}\,\frac{e\,E^*}{\hbar\,\varepsilon^{1/2}}\,\frac{d}{d\varepsilon}\left(\varepsilon^{3/2}\,g_e\right) = \frac{\partial f_o}{\partial t} \tag{2.31}$$

$$\frac{-g_e}{\tau} - \frac{heE}{m^*} = \frac{\partial g_e}{\partial t} \tag{2.32}$$

where E^* is the total field (applied d.c. and microwave electric fields). If the microwave field is parallel to the d.c. field the total field can be expressed as

$$E^* = E_o^*\,(1 + \lambda\, e^{i\omega t}) \tag{2.33}$$

where λ is a constant which is much smaller than unity for small signal analysis. By setting

$$\begin{aligned} f_o &= f_{os} + \lambda f_1\, e^{i\omega t}\,, \\ g_e &= g_{es} + \lambda g_1\, e^{i\omega t} \end{aligned} \tag{2.34}$$

where f_{os}, g_{es}, f_1, and g_1 are constants independent of time. Using the above equations, we obtain by neglecting 2nd order term in λ the following

$$\left(\frac{\partial f_{os}}{\partial t}\right)_c - \frac{eE_o^*}{\hbar}\left(g_{es} + \frac{2}{3}\,\varepsilon g_{es}'\right) = 0 \tag{2.35}$$

$$g_{es} = -\,\frac{h\,eE_o^*\,\tau}{m^*}\,f_{os}', \tag{2.36}$$

$$\left(\frac{\partial f_1}{\partial t}\right)_c - \frac{2}{3}\,\frac{e\,E_o^*}{\hbar}\,\frac{1}{\varepsilon^{1/2}}\,\frac{d}{d\varepsilon}\left[\varepsilon^{3/2}(g_{es} + g_1)\right] = i\omega f_1 \tag{2.37}$$

$$g_1 = \frac{-he\,E_o^*\,\tau}{m^*(1 + i\omega\tau)}\left(\frac{\partial f_{os}}{\partial t} + \frac{\partial f_1}{\partial \varepsilon}\right) \tag{2.38}$$

It is clear that Eqs. (2.35) and (2.36) represent the d.c. components of Eqs. (2.29) and (2.30). They have been solved to various degrees for n-Ge by Reik and Risken [51], and Yamashita and Inoue [69]

taking into account the optical and acoustic scattering in $(\frac{\partial f_{os}}{\partial t})_c$.

Nag and Das [42] have obtained a solution of Eqs. (2.37) and (2.38) for n-Ge at a field of 2 KV/cm assuming isotropic effective mass, acoustic and optical phonon scattering, and using various values for interaction constants. Their analysis is successful in explaining the d.c. curves; and the agreement between their theory and experiment is fairly good for changes of σ but comparatively poor for changes of ε.

To assess the effect of inter-electronic scattering on hot-electron microwave conductivity, Guha and Nag [23] have recalculated the results of Gibson et al [21] taking the effect of anisotropic effective mass into account, but assuming that the inter-electronic scattering establishs a Maxwellian distribution. They have shown that experimental results on the microwave incremental conductivity agree with the theory based on a displaced Maxwellian distribution and the analysis by Nag and Das [42], and calculated that the conductivity is not sensitive to inter-electronic scattering because the effect of anisotropy in the band structure is small at room temperature.

For a more accurate solution of the Boltzmann equation Budd [39] converts the Boltzmann equation into an integral equation with time and position variables measured along the collison-free trajectories of the carriers. He has solved the Boltzmann equation for P-Ge using this method. The theoretical analysis agrees quite well with experimental results. Law and Kao [38] have also presented a new approach to the exact analytical solution of the time dependent Boltzmann transport equation by means of an iterative perturbation technique for single-valley semiconductors, and give examples to demonstrate the use of their method to predict a.c. and d.c. conductivities in nondegenerate single-valley semiconductors.

CHAPTER 3

EXPERIMENTAL TECHNIQUES

3.1. *Measurement of Microwave Properties Using a Slotted Waveguide Structure.*

Semiconductor properties may be measured at microwave frequencies by inserting a suitable sample, normally a rectangular slab in a waveguide [11, 21, 24, 39]. The conductivity and permittivity are deduced by measuring the propagation coefficient corrected for an inhomogeneously filled waveguide. This method is straightforward provided that the sample is in contact with at least two of the waveguide walls. In the measurement of hot-electron effects, a direct voltage is applied to the sample, and in this case the sample has to be insulated from the waveguide walls. It is also desirable to keep the contacts on the sample outside the waveguide, to avoid difficulties arising from carrier injection. In this situation some principal effects such as those arising from the presence of the slot and the finite length of the sample have to be considered [25].

3.1.1. *Inhomogeneously filled waveguide.*

In the following discussion it will be assumed, in order to simplify calculations that the dielectric loss is very small and may be neglected. For semiconductors, however, the permittivity ε_r will be replaced by the complex permittivity $\varepsilon_r^* = \varepsilon' - j\varepsilon''$.

The normal modes of propagation for guides loaded with dielectric slabs are generally not either E or H modes, but a combination of E and H modes. An exception is the case of H_{no} modes which have

the electric field parallel to the slab and no variation of field along the dielectric-air interface.

For an asymmetrically loaded guide as illustrated in Fig. 3.1, with a slab whose relative dielectric constant is ε_r, the relation between the two wave numbers K_{1n} in air and K_{2n} in the dielectric can be determined from the transcendental equation [11, 39],

$$K_{1n} \tan K_{2n} t = - K_{2n} \tan K_{1n} d \tag{3.1}$$

where t is thickness of the slab. The eigenvalue of Eq. (3.1) may be obtained directly by considering the transverse plane equivalent circuit of the loaded guide as illustrated in Fig. 3.2. The equivalent transmission-line circuit is a junction of two lines, with characteristic impedances proportional to the wave impedances (inversely proportional to the wave numbers) of the two sections, terminated by short-circuits at opposite ends. The wave numbers K_{1n} and K_{2n} are determined from the condition that the zero impedance load at $x = a$ must transform to a zero impedance at $x = o$. On the basis of conventional transmission-line theory we have

$$Z_{in} = \frac{1}{K_{1n}} \frac{i\, K_{2n}^{-1} \tan K_{2n} t + i\, K_{in}^{-1} \tan K_{1n} d}{K_{1n}^{-1} - K_{2n}^{-1} \tan K_{2n} t \tan K_{1n} d} \tag{3.2}$$

The condition that Z_{in} should equal zero is in fact that given by Eq. (3.1). This transverse-resonance procedure is useful for finding eigenvalue equations for guides loaded with several dielectric slabs.

The eigenvalue equation for LSE modes for an inhomogeneously but symmetrically filled guide, as illustrated in Fig. 3.3, which is usually used in the measurement of semiconductor properties, can be obtained from the condition that a short circuit should appear at the

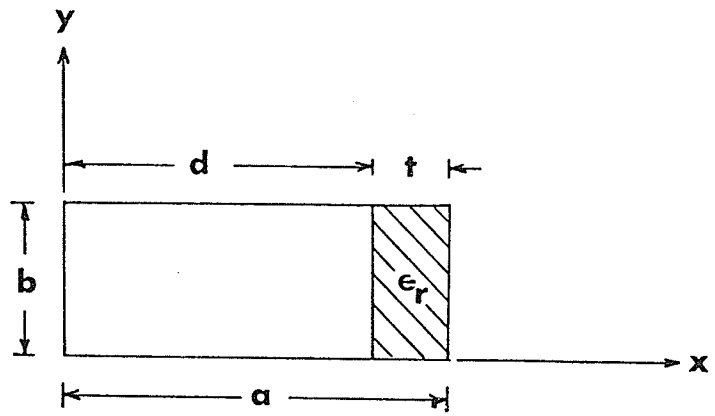

Fig. 3.1. Asymmetrical dielectric slab-loaded guide

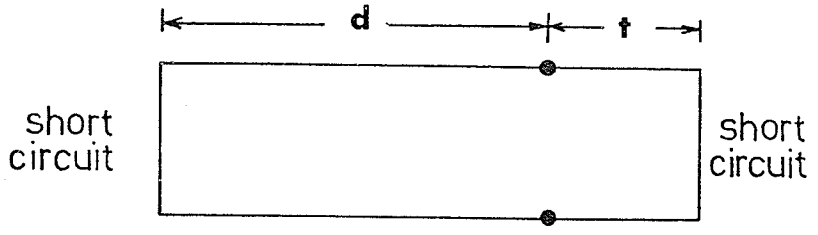

Fig. 3.2. Transverse equivalent transmission-line circuit

centre of the slab for asymmetrical modes and an open circuit for symmetrical modes. The corresponding eigenvalue equations for these two cases are given by

$$K_{2n} \tan K_{1n} d = K_{1n} \tan \frac{K_{2n} t}{2} \tag{3.3}$$

$$K_{1n} \cot K_{1n} d = K_{2n} \tan \frac{K_{2n} t}{2} \tag{3.4}$$

Symmetric modes are those which have a symmetrical variation of E_y with respect to x about the point $x = a/2$.

The relationship between the propagation constant in the Z direction and the transverse wave vectors is

$$\begin{aligned} \gamma^{*2} &= K_{1n}^2 + \left(\frac{m\pi}{b}\right)^2 - K_o^2 \\ &= K_{2n}^2 + \left(\frac{m\pi}{b}\right)^2 - \varepsilon_r^* K_o^2 \end{aligned} \tag{3.5}$$

Equation (3.4) for the H_{10} mode can be written as

$$\frac{\tan[(\gamma^{*2} + K_o^2)^{\frac{1}{2}} (\frac{a - t}{2})]}{(\gamma^{*2} + K_o^2)^{\frac{1}{2}}} = \frac{\cot[(\gamma^{*2} + \varepsilon_r^* K_o^2)^{\frac{1}{2}} t/2]}{(\gamma^{*2} + \varepsilon_r^* K_o^2)^{\frac{1}{2}}} \tag{3.6}$$

This equation has been used by Gunn [24], Gibson et al [21] and Wu et al [68] for measuring the complex permittivity of n-Ge, n-Si, and n-GaAs.

3.1.2. *The dielectric step discontinuity*

So far only the ideal case in which the dielectric slab is assumed to be infinite in length has been considered. For a dielectric step discontinuity the Rayleigh-Ritz [11] method may be employed to obtain an approximate solution for the equivalent circuit of the junction of an empty and inhomogeneously filled rectangular waveguide

shown in Figs. 3.4 and 3.5. As an example, the parameters for an equivalent circuit, see Fig. 3.6, with $K_o^2 = 4$, $\varepsilon_r = 2.56$, $a = 0.90$ inches, and t ranging from 0 to 0.5 inches, have been computed and plotted as functions of t/a. The turns ratio $n:1$ is equal to unity for all values of t. The series reactance X_1 is very small, while the shunt reactance X_2 is large. For all practical purposes, the equivalent circuit is just a junction of two transmission lines, with characteristic impedances proportional to the wave impedances of the H_{10} mode in the two regions.

3.1.3. *Propagation constants of the loaded guide.*

Using measurements from a transmission bridge Gunn [24] has obtained γ^* from

$$\gamma^* = \alpha + j\beta = \left| \frac{\Delta A}{(\ell_1 - \ell_2)\ 8.686} \right| + j \left| \frac{\Delta \phi}{(\ell_1 - \ell_2)\ 97.3} \right| \qquad (3.7)$$

where $\Delta\phi$ and ΔA are, respectively, the phase and attenuation change between two identical samples except for differing length, ℓ_1 and ℓ_2. From Eqs. (3.6) and (3.7) we can determine ε_r^*.

The same technique has been used for a completely filled waveguide section by Westphal [67]. If ΔA is given in dB, and $\Delta\phi$ in degrees, the attenuation and phase constants of the sample filled guide are

$$\alpha = \frac{\Delta A}{8.68\ \Delta \ell} \qquad \text{Nepers/unit length} \qquad (3.8)$$

$$\beta = \frac{\Delta \phi}{57.296\ \Delta \ell} + \frac{2\pi}{\lambda_1 \Delta \ell} \qquad \text{radians/unit length} \qquad (3.9)$$

where $\Delta \ell = \ell_1 - \ell_2$. The only difficulty of this method is that it

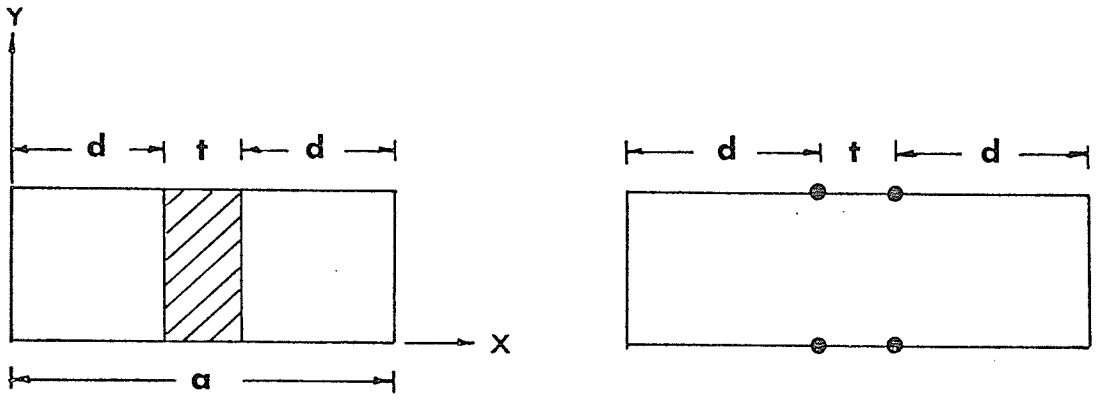

Fig. 3.3. Symmetrical dielectric slab-loaded guide and its transverse equivalent transmission-line.

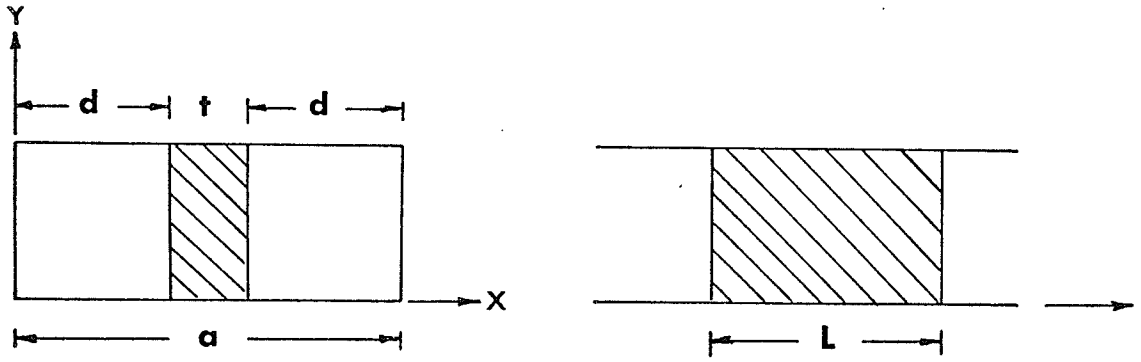

Fig. 3.4. The dielectric step discontinuity.

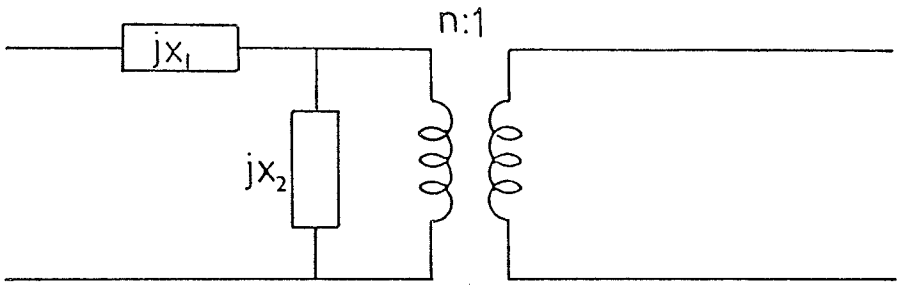

Fig. 3.5. Equivalent circuit for the dielectric step

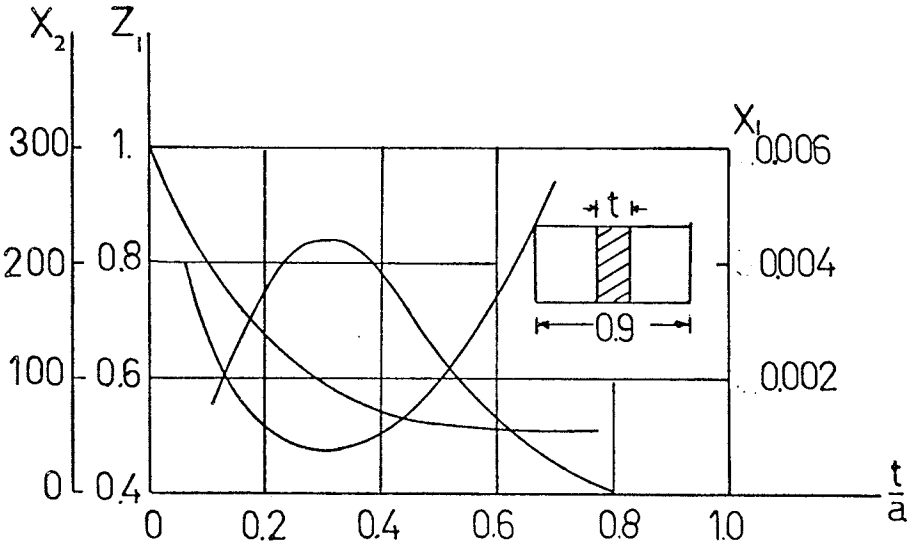

Fig. 3.6. Equivalent-circuit parameters for the dielectric step. $\varepsilon_r = 2.56$, $K_o = 2$ rad./cm.

requires two samples with exactly the same electrical properties and cross-section. This is usually not easy to obtain and also the uncertainties arising from multimeasurements increase.

Considering the multiple reflections at the interfaces between the loaded and air filled section of waveguide, Wu et al [68] have determined the transmission coefficient T^*. It is given by

$$T^* = e^{-(A + j\phi)} = \frac{4\,\gamma_o^*\,\gamma^*\,e^{-(\gamma^* - \gamma_o^*)\ell}}{(\gamma_o^* + \gamma^*)^2 - (\gamma^* - \gamma_o^*)^2\,e^{-2\gamma^*\ell}} \qquad (3.10)$$

The propagation constant γ^* can be found from Eq. (3.10) either by graphical means by plotting A and ϕ as functions of γ^*, or by numerical computation methods. The latter technique was adopted by Wu who used a Newton-Raphson iteration technique.

3.1.4. *Corrections required for a slotted waveguide system*

The practical waveguide circuit, shown in Fig. 3.7 differs from the idealized model in three significant respects.

a) Reflections occur at each end of the sample and must be considered when calculating the propagation-coefficient from the measured values of attenuation and phase.

b) The slots disturb the field pattern within the waveguide so that the propagation constant is no longer related exactly to the semiconductor properties by Eq. (3.6).

c) Additional reflections may occur at the ends of the slotted section, causing measurements of attenuation and phase to depend on the longitudinal position of the sample in the slot.

The approach used by Gunn [25] was to extend the range of measurements made on the semiconductor, to permit extrapolation to the

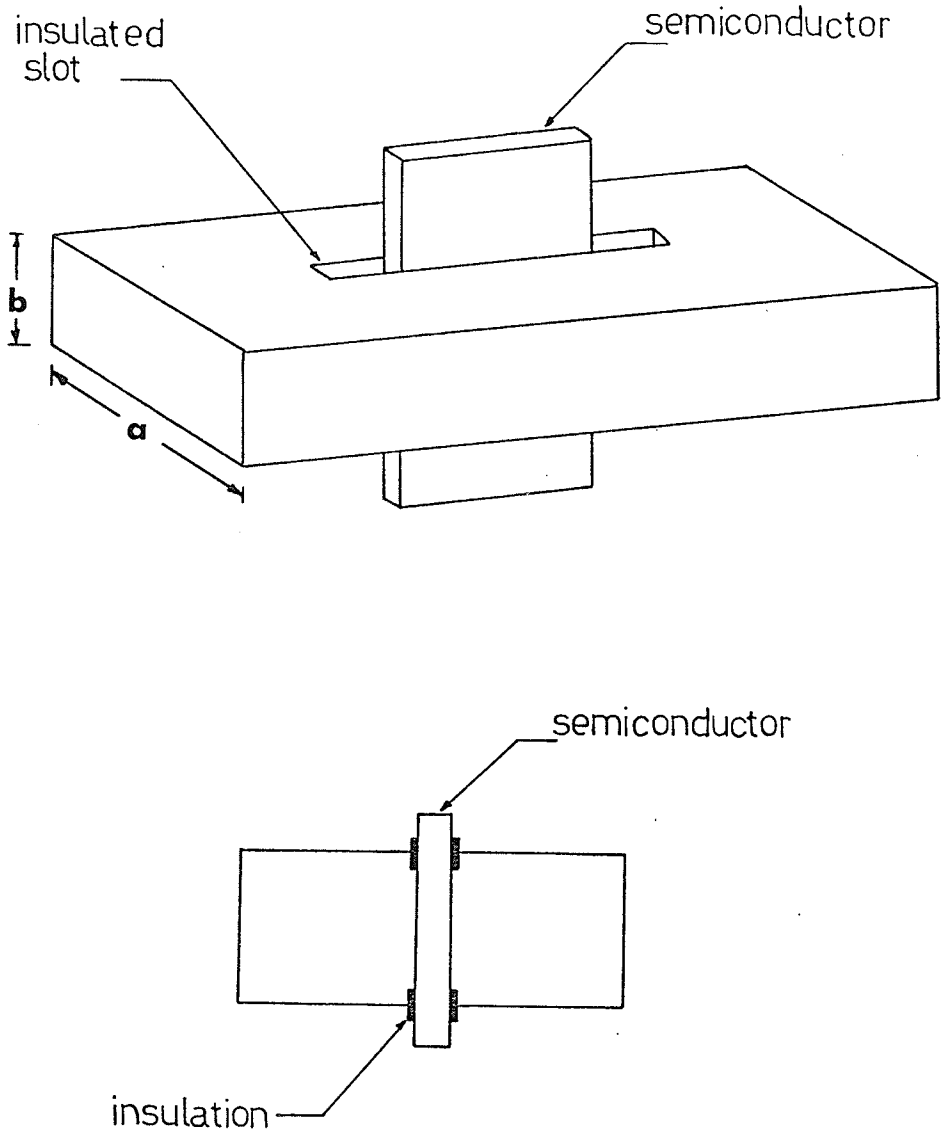

Fig. 3.7. Practical waveguide circuit.

ideal case considered above. The techniques so far described are aimed at providing an accurate estimate of the propagation coefficient γ^* and hence of the complex permittivity. To take into account the end effects Gunn has deduced the following equation

$$\gamma^* = \frac{1}{\ell_1} \cosh^{-1} \frac{T_2(T_1 + T_3)}{2T_1 T_3} \tag{3.11}$$

where T_1 is the complex wave transmission coefficient corresponding to a sample of length ℓ, T_2 corresponding to a sample of length $\ell + \ell_1$, and T_3 to length $\ell + 2\ell_1$. He has suggested that for practical systems it is desirable to use long samples and to derive the propagation coefficient of the inhomogeneously filled section from the slopes of straight sections off graphs plotted against ℓ.

The effect of the insulated slots can be determined by measuring the dependence of the propagation coefficent of a slotted guide on its b dimension [25, 39]. The correction procedure to allow for the presence of the slot is based on the fact that the effect of the slot is likely to be localized near the two broad walls of the guide. As the separation b between these walls is increased the change in propagation conditions caused by the slots will decrease and in the limit, when b tends to infinity, its behaviour will be essentially the same as for the ideal case. This suggests that the propagation coefficient γ^* for the slotted section will differ from the propagation coefficient γ' for the corresponding geometry without slots by a correction term which tends to zero as b tends to infinity. This relation may be expressed in the form

$$\gamma^* = \gamma' + \frac{K_1}{b} + \frac{K_2}{b} + \ldots . \tag{3.12}$$

For the first approximation Eq. (3.12) can be written as

$$\gamma^{*} = \gamma' + \frac{K_1}{b} \tag{3.13}$$

The constant K_1 is likely to be complex since the region of the slot contains semiconductor which absorbs energy. Eq. (3.13) may thus be split into real and imaginary parts as

$$\alpha = \alpha' + \frac{K'}{b} \tag{3,14}$$

$$\beta = \beta' + \frac{K''}{b} \tag{3.15}$$

where α' and β' are, respectively, the attenuation and phase change coefficients for the ideal waveguide structure without slots and α and β are the corresponding one's for the slotted guide with height b. The values of the constants K' and K'' can be obtained by performing a series of measurements on waveguides with different heights.

The section of waveguide containing the slot and the semiconductor sample forms a complicated transmission system of which the measured attenuation and phase are functions of the position of the sample in the slot and the magnitude of the attenuation. To avoid an apparent decrease in attenuation produced by the slot coupling, the slot should be short, or the sample should be located in a position close to one end of the slot. The magnitude of the slot-coupling effect depends on the physical dimensions of the slot and the thickness of the insulant [46].

3.2. *Measurements of Microwave Properties Using Slotted Coaxial Line*

Many techniques are available for the measurements of dielectric properties of materials using the slotted line [5, 37, 64, 64a]. Different sample shapes have been used for these techniques and Fig. 3.8 shows

two such shapes. For the materials under investigation a technique using a capacitive sample holder which terminates the slotted line is found to be the most suitable. A restriction results for the other methods from the difficulty of producing suitable samples. Hence, this technique will be presented in detail.

A small shunt capacitor terminating a coaxial transmission line section is used as a sample holder, as shown in Fig. 3.8. The equivalent circuit of this sample holder is a capacitor of capacitance $C = \varepsilon_r^* C_o$ [30], where ε_r^* is the relative complex permittivity of the material filling the test capacitor, which can be calculated from the measured input reflection coefficient at any desired frequency and temperature, provided that the geometrical dimensions of the capacitor are much smaller than the wavelength.

Stuchly et al [64] have found the relation between the optimum capacitance of the empty sample holder C_o and frequency for lossless materials. This relation is

$$\frac{Z_c}{Z_o} = \varepsilon' \qquad (3.16)$$

where $Z_c = \frac{1}{\omega C_o}$ is the impedance of the empty capacitor, and Z_o is the characteristic impedance of the coaxial line. They have obtained the optimum capacitance of an empty sample holder for any frequency in the range of 10 MHz to 10 GHz.

3.2.1. Voltage standing wave ratio measurement.

Several methods are available for the measurement of voltage standing wave ratio [VSWR] in a transmission line using a standing wave indicator [5, 37, 46, 52, 64a]. The choice of the method is dependent

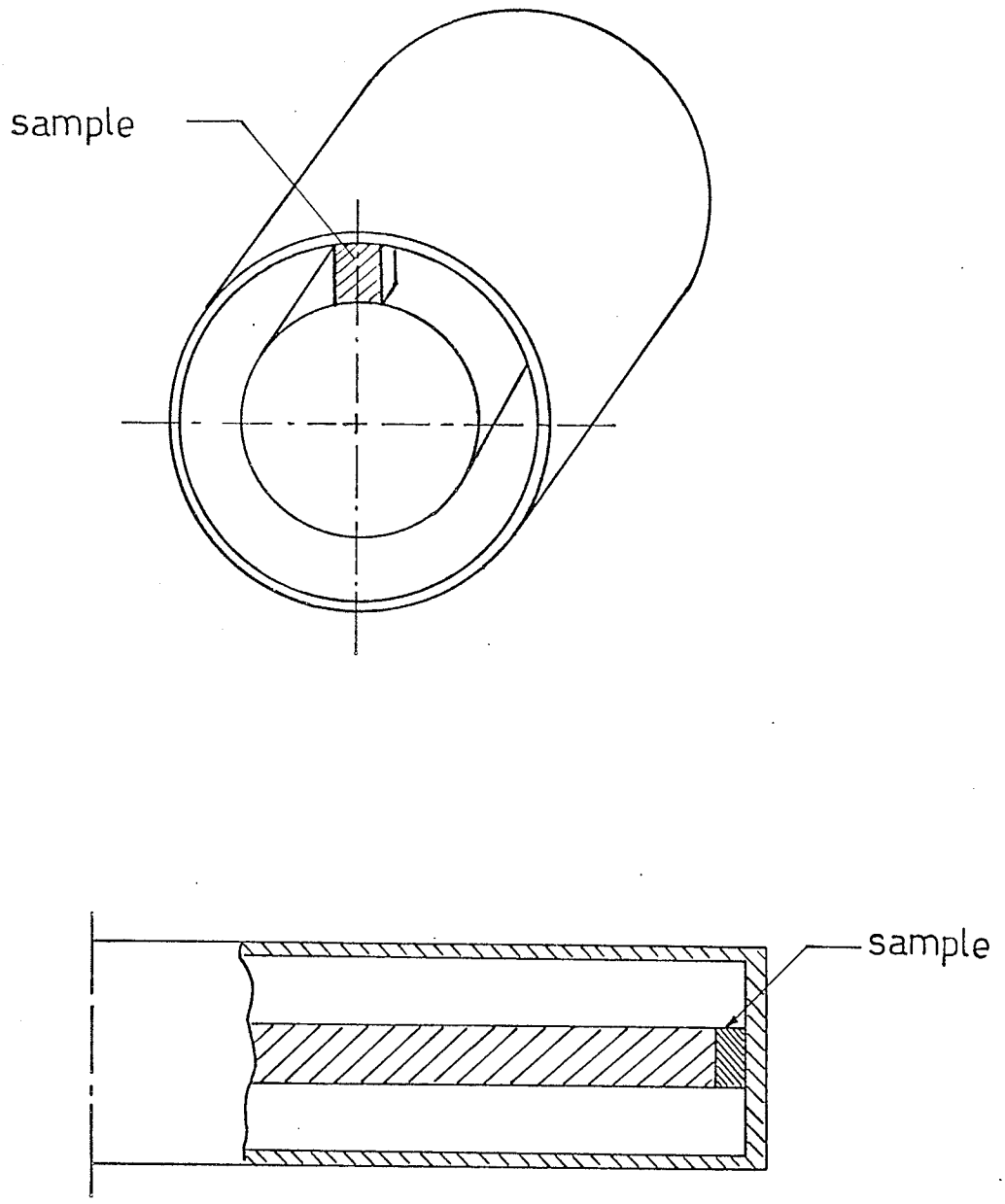

Fig. 3.8. Two different sample shapes used in conjunction with coaxial line techniques.

on the expected magnitude of the VSWR, the degree of sophistication required to reduce the errors of the measurement to an acceptable minimum, and the conditions imposed by the nature of the experiment. When the VSWR is large, the method of Roberts and Von Hippel [6, 41, 52] is employed. The procedure is to measure the distance between two points on either sides of the minimum at a level of field strength which is an arbitrary multiple M of the minimum field strength. This is shown in Fig. 3.9. If the measured width is W, then the standing wave ratio can be found from the equation

$$S^2 = \frac{M^2 - \cos^2(\frac{\pi W}{\lambda_g})}{\sin^2(\frac{\pi W}{\lambda_g})} \tag{3.17}$$

where S is the VSWR, and λ_g is the guide wavelength. For minimum error it can be shown [20] that M must be selected such that

$$M = \frac{2S^2}{S^2 + 1} \tag{3.18}$$

In order to determine M accurately, precise knowledge of the minimum field strength is essential. However, in experiments where the VSWR is very large or where the incident field strength is very low, this minimum may approach the general noise level of the detector system and may even fall below it. As a result, the errors in establishing M could become extremely large. A method which overcomes this problem by specially avoiding measurements in the noise region at the minimum, is proposed by Owens [46]. The procedure, as indicated in Fig. 3.10, is to choose a convenient level of field strength just above the noise level and to note the distance W_1 between points on each side of the minimum at this level and then repeat for a field strength M times the first one to find the seperation W_2. The equation

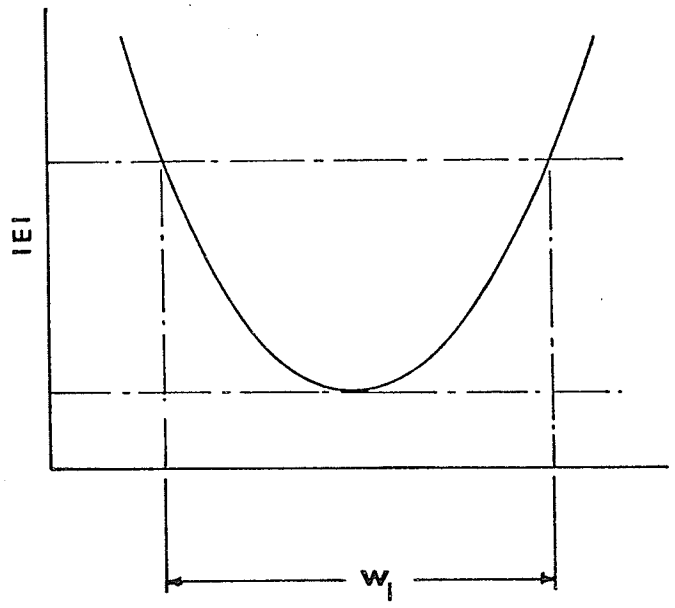

Fig. 3.9. Standing wave pattern for E_{min} above noise level.

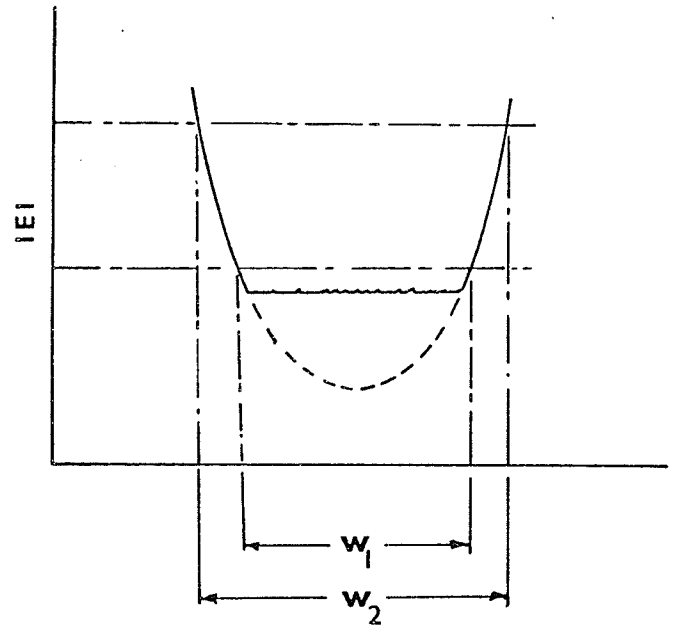

Fig. 3.10. Standing wave pattern for E_{min} below noise level.

$$S^2 = 1 + \frac{M^2 - 1}{\sin^2(\frac{\pi\omega_1}{\lambda_g}) - M^2 \sin^2(\frac{\pi\omega_1}{\lambda_g})} \tag{3.19}$$

is used for calculating the standing wave ratio.

The main advantage of both methods is that measurements are concentrated around standing wave minima where the total field is low, so that, although the probe coupling is appreciable, the influence of the probe is very small.

3.2.2. *Line attenuation errors.*

Line attenuation presents a fundamental limitation to the accurate measurement of VSWR of a transmission-line load. An expression for VSWR at any point on the line is given by [5]

$$\frac{1}{S} = \tanh[\tanh^{-1}\frac{1}{S_L} + \alpha\ell] \tag{3.20}$$

where α is the line attenuation in nepers/meter; ℓ is the distance from the point at which the VSWR is measured to the load reference plane and S_L is the standing wave ratio at the load. For high VSWR's and low loss lines, i.e.: $\frac{1}{S_L} \ll 1$ and $\alpha\ell \ll 1$, we obtain

$$\frac{1}{S} \simeq \frac{1}{S_L} + \alpha\ell \tag{3.21}$$

If the line is terminated in a perfect short then

$$\alpha\ell = \frac{1}{S_o} \tag{3.22}$$

where S_o is the short circuit VSWR. Hence, as a first order correction for VSWR for small line attenuation, we can use the equation

$$\frac{1}{S} \simeq \frac{1}{S_L} + \frac{1}{S_o} \tag{3.22}$$

to find the corrected VSWR at any point on the line.

CHAPTER 4

EXPERIMENTAL PROCEDURES

The two experimental techniques presented in Chapter 3 were used in this investigation. The transmission bridge technique was used to measure permittivity over the frequency range 29 to 31 GHz and the slotted line technique at a lower frequency range from 1 to 4 GHz. The second technique allows application of bias field up to 25 KV/cm whereas the field as applied in conjunction with the first technique is limited to a maximum of 3.5 KV/cm.

4.1. *Sample Preparation*

The material used in this experimental work is a chalcogenide alloy $Si_{12} - Ge_{10} - As_{30} - Te_{48}$ and undoped anthracene crystals.

Samples used for the two experimental techniques differ only in the final shape and dimensions, but not in the main procedure of sample preparation.

The amorphous alloy was supplied by Malven Radar Research Laboratories in England and received in the form of an ingot, approximately 3 cm in length and 1 cm in diameter. The basic steps in producing samples from the bulk material are outlined as follows:

The ingot was cut into wafers with a precision diamond wheel cutter, each wafer being approximately 1mm in thickness. It was found that this thickness is adequate to allow handling and machining of the sample without breaking it. A diamond edge cutter was used to cut the wafers into rectangular shapes approximately 7 x 7 mm, to be used with the transmission bridge technique. An ultrasonic cutting machine was used

to cut the wafers to smaller diameters of 6,5 mm with a specially designed cutting cylinder with an inner diameter of the same dimension, This diameter is slightly larger than the diameter of the sample mount terminating the slotted line. This diameter increase is needed in order to prevent surface breakdown at the sides of the sample.

To reduce the thickness of the sample to the desired thickness of about 350 microns for each technique, each sample was mounted on a brass block using wax as an adhesive. Care had to be taken at this point not to subject the sample to excessive heat for this could result in localized regions of recrystallization. The brass block was heated to the melting temperature of wax, and once the sample had been placed into position the entire assembly was quickly cooled to room temperature. The exposed side of the sample was then polished to reduce the sample thickness by about 200 microns. After one surface had been polished the sample was removed and remounted on the brass block so that the other surface could be polished. This final polishing step was used to reduce the sample thickness to the desired value. It was then removed from the brass block and placed in warm trichloroethylene to remove wax, finger-prints, dirt and other foreign substances from its surface. To avoid any kind of chemical reaction between the sample and trichloroethylene, the sample was subjected to cleaning for not more than five to ten minutes and then transferred to methanol.

It should be mentioned here that this amorphous material is extremely brittle; a property which limits the thickness of the sample to the above mentioned values. It was found that reducing the thickness any further would cause breakage of the sample.

The anthracene crystals were supplied by Harshaw Chemical Company.

The bulk anthracen was cleaved parallel to the a-b plane to a thickness of about 5 mm. It was impossible to start with an initial sample thickness of less than 5 mm without breaking the sample. The thickness was reduced by polishing the sample very slowly with a smooth cloth dampened with pure benzine. Care was taken in order not to damage the crystal by overheating or introducing lattice dislocations. It was then cut to either a rectangular shape using a very sharp knife, or to a circular shape using a specially designed sharp cutter in the shape of a cylinder of proper diameter.

4.2. *Transmission Bridge*

The transmission bridge provides a convenient means of measuring the propagation coefficient of the section of the guide containing the dielectric material as adjustments of the attenuation and phase standards are largely independent. The bridge circuit used is based on two 10dB broadband directional couplers [Hitachi, model R2101-10] of directivity better than 35 dB. The circuit diagram for the bridge is shown in Fig. 4.1. The matched isolator assembly in the top bridge arm reduces the possibility of reflections from the sample entering the lower arm or being returned to the sample. It consists of an isolator [Hitachi model R1901] of minimum isolation of 20 dB and an E-H tuner which can compensate to within a VSWR of 1.02, for a mismatched load having a VSWR as high as 10.1 to 20.1. The lower bridge arm consists of a precision direct reading attenuator of the range 0 to 50 dB and accuracy 0.1 dB or $\pm$1% of reading, whichever is greater, and a precision direct reading phase shifter [TRG model A528] of 0.6 dB insertion loss. Two variable attenuators, [Hitachi model R1525] of 0 to 30 dB attenuation range are

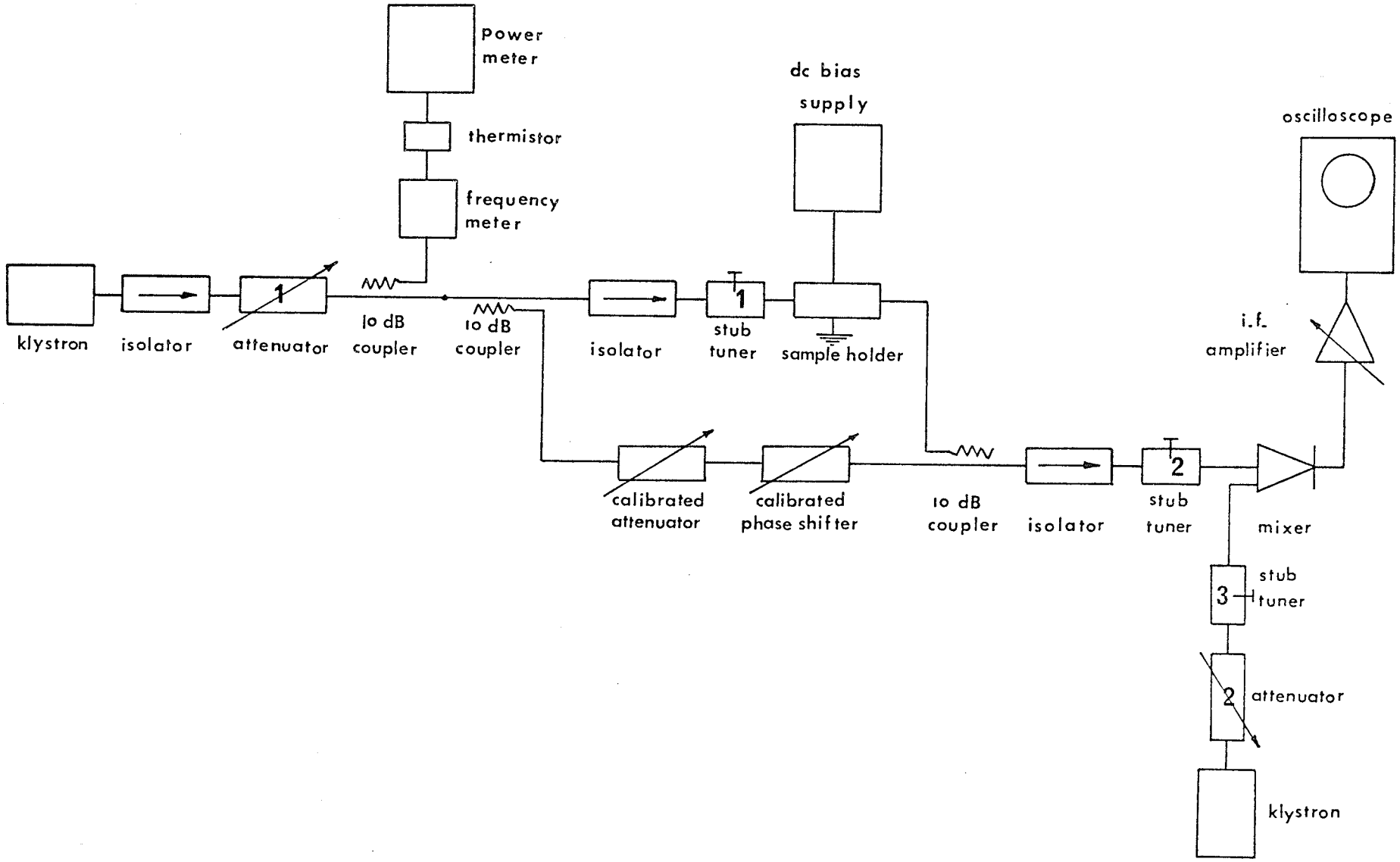

Fig. 4.1. Transmission bridge circuit diagram

used to control the output of both Klystons. Two Klystrons [OKI model 30V10] are used respectively as a signal oscillator and local oscillator. They have a frequency range from 28 - 32 GHz with a minimum output power of 100 mW. The mixer preamplifier [Varian model KGT-7-60-20-50] has an i.f. frequency of 60 MHz, a 3 dB bandpass of 24.0 MHz and a power gain (rf to If) of 23.5 dB. The i.f. amplifier has a bandwidth of 20.5 MHz and adjustable gain of from 20 to 81 dB. The frequency of the signal oscillator is measured by means of a broadband direct reading frequency meter [Hitachi model R2210] with a 10 MHz minimum scale division and accuracy of $\pm$0.14%. The detector is an oscilloscope [Tektronix, model 454] having a bandwidth of 150 MHz.

A closed water cooling system is used to keep the klystrons at constant temperature and hence maintained at stable frequency operation. The system consists mainly of a portable coolant pump [Narda model 58Z2] and two copper tubes of $\frac{1}{8}$ inch diameter which are wound around each klystron, as shown in Fig. 4.2. This cooling system has proved to be very satisfactory with the klystrons reaching stable frequency operation in about 20 minutes.

4.2.1. *Measurement procedure.*

The measurement procedure can be divided into steps as follows:

1. After the equipment was switched on for approximately 20 minutes the signal klystron was adjusted to the proper frequency, and checked with the wavemeter. The local oscillator was then adjusted to present maximum undistorted signal output on the oscilloscope screen. This is an indication that a difference frequency of 60 MHz has been obtained.

2. The tuners in various parts of the circuit were adjusted to

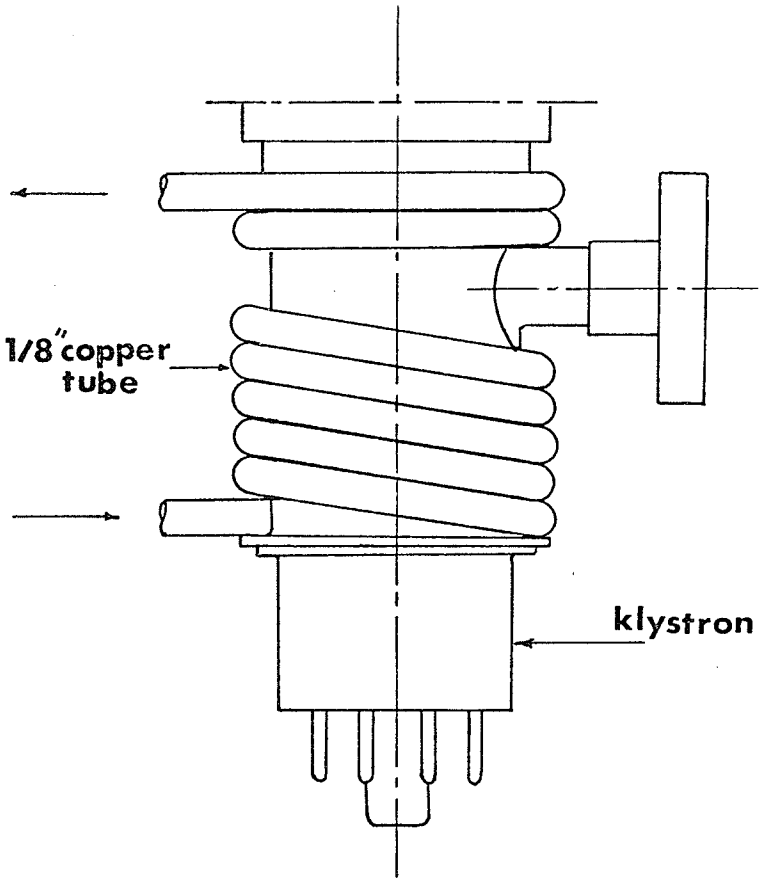

Fig. 4.2. Cooling mount of klystrons

initially provide matched conditions. Tuner 3 was adjusted for maximum crystal current output and attenuator 2 set to maintain a crystal current level of 0.2 mA, which was chosen experimentally so as to provide linear mixing. When matching the local oscillator arm, attenuator 1 was set to its maximum value for a minimum signal to the mixer.

3. To match the rest of the circuit, the attenuation level was reduced in attenuator 1, then the calibrated attenuator in the lower arm was set to maximum so as to isolate the lower arm and permit adjustment to tuner 1 to obtain a matched condition between the isolator and the sample holder. The circuit was matched when tuners 1 and 2 were so set that the i.f. output is a maximum. Tuners 1 and 2 could be left unchanged, but tuner 1 required adjustment with each change in sample measurement conditions. When performing measurements attenuator 1 should be reduced to a low level to ensure sufficient detection system sensitivity. Another factor which has to be taken into consideration when setting this level is the maximum power level of 3 mW which can be absorbed by the thermistor used in conjunction with the wavemeter.

4. The system was then ready for taking measurements. The attenuation A and phase shift ϕ_1 were noted for the empty sample holder at bridge balance. The sample was then introduced with bias field E, and readings A_2 and ϕ_2 noted. The attenuation and phase shift due to the sample under bias conditions is then given by $A = A_2 - A_1$ and $\phi = \phi_2 - \phi_1$. These parameters can then be processed as discussed in Chapter 3 to give the complex permittivity of the sample.

4.2.2. *Sources of errors*

1) Instrument errors: The precision attenuator has some parasitic

phase shift which varies with attenuator setting and the small attenuation characteristic associated with the calibrated phase shifter also changes with its setting. However, A and ϕ are only relative readings so errors due to this source are negligible.

2) Deviation from theoretical conditions: The equations used to derive the complex permittivity were obtained assuming ideal conditions; i.e., no reflection at the slot edges and only the dominant mode propagating in the sample holder guide. This assumption is estimated to be a few percent off the real physical situation [68].

3) Human Factor: Errors arising from the fact that the bridge balance depends on the balance observed on the oscilloscope screen, which in turn is being judged by the human eye. Also, all readings of attenuation and phase shift are taken from instrument scales. These errors can be minimized by repeating measurements and averaging the readings so obtained.

4.3. *Slotted Coaxial Line Technique.*

The equipment arrangements used consists of a precision slotted-line terminated by a specially fabricated coaxial line mount containing the sample. The superhetrodyne detection technique was used because of its greater sensitivity. Measurements were made over the frequency range 1 to 4 GHz.

A block diagram of the experimental arrangements is shown in Fig. 4.3. It consists of a precision slotted-line [Alford 2382A-4] operable in the frequency range 0.4 to 4 GHz, a signal oscillator [H.P. 8690A main frame sweep oscillator with H.P. 8699B plug in unit with a frequency range 0.1 - 4 GHz], and a precision test receiver

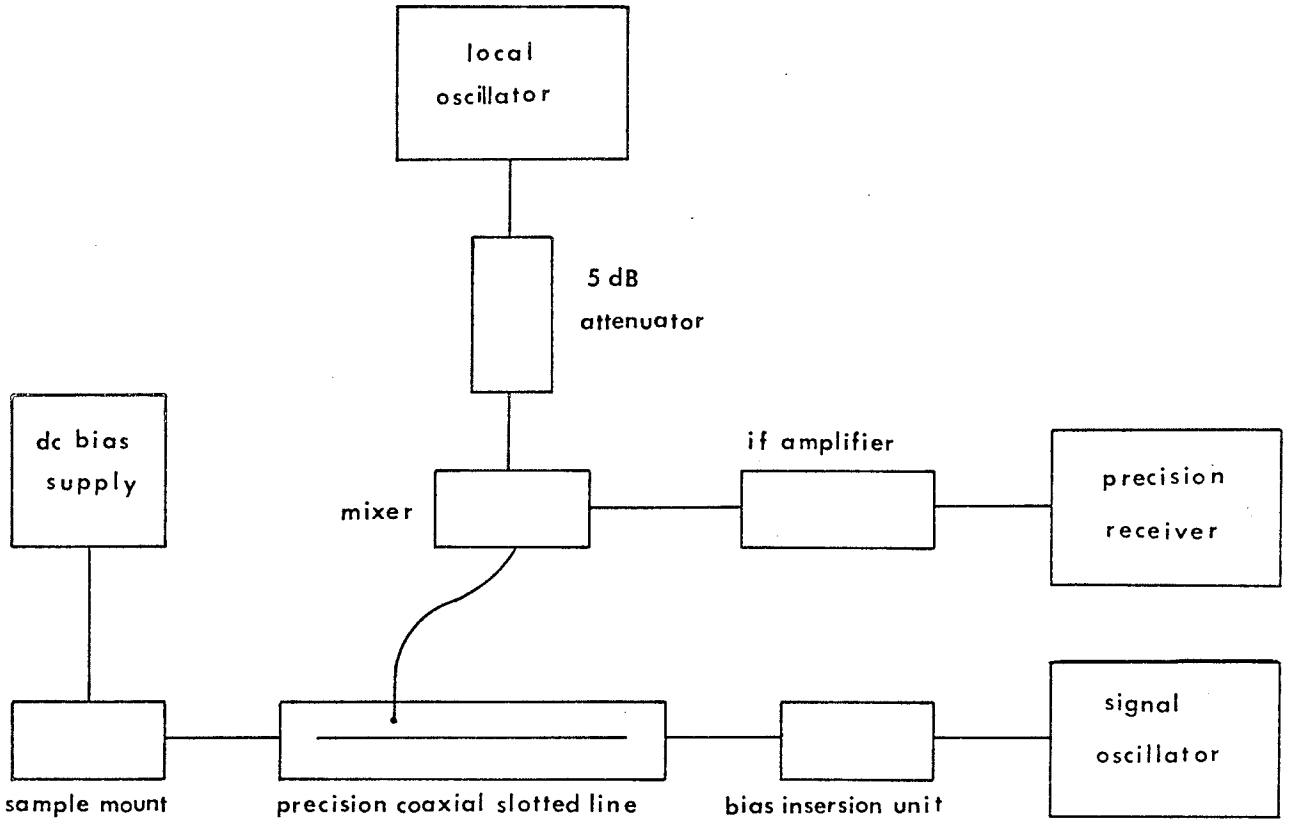

Fig. 4.3. Coaxial line technique circuit diagram.

[Airborn type 132, with Type 132 preamplifier]. A biasing insersion unit [GR 874-FBL] was used to provide the d.c. connection between the inner and outer conductor of the slotted line, and a unit oscillator [GR type 1218A] served as the local oscillator for the range 0.9 - 2 GHz and a signal source [H.P. model 8616B] for the frequency range 1.8 - 4.5 GHz.

4.3.1. *The sample holder.*

A specially fabricated mount was used for these measurements and is shown in Fig. 4.4. It was designed to allow application of the d.c. biasing voltage. The wide flanges, isolated by a 20 micron thick mica sheet, introduce a very large capacitance compared to that of the sample. Fig. 4.5 shows the mount construction. To permit measurements of permittivity at different temperatures, a copper tube of $\frac{1}{8}$ inch diameter was wound in a spiral shape and attached to the sample holder as shown in Fig. 4.6. The mount temperature was charged by passing hot water through the tube.

4.3.2. *Measurement procedure*

1. The equipment was switched on for about 45 minutes to allow it to warm up and reach stable conditions. The frequency of the main oscillator was adjusted first to the desired frequency. The frequency of the local oscillator is then set 30 MHz below this frequency. This condition is detected by obtaining a maximum at the receiver meter. The level of the local oscillator is set to give a mixer current of between 0.2 - 1 mA which insures linear mixing conditions.

2. The load reference plane was first found. The center rod of the

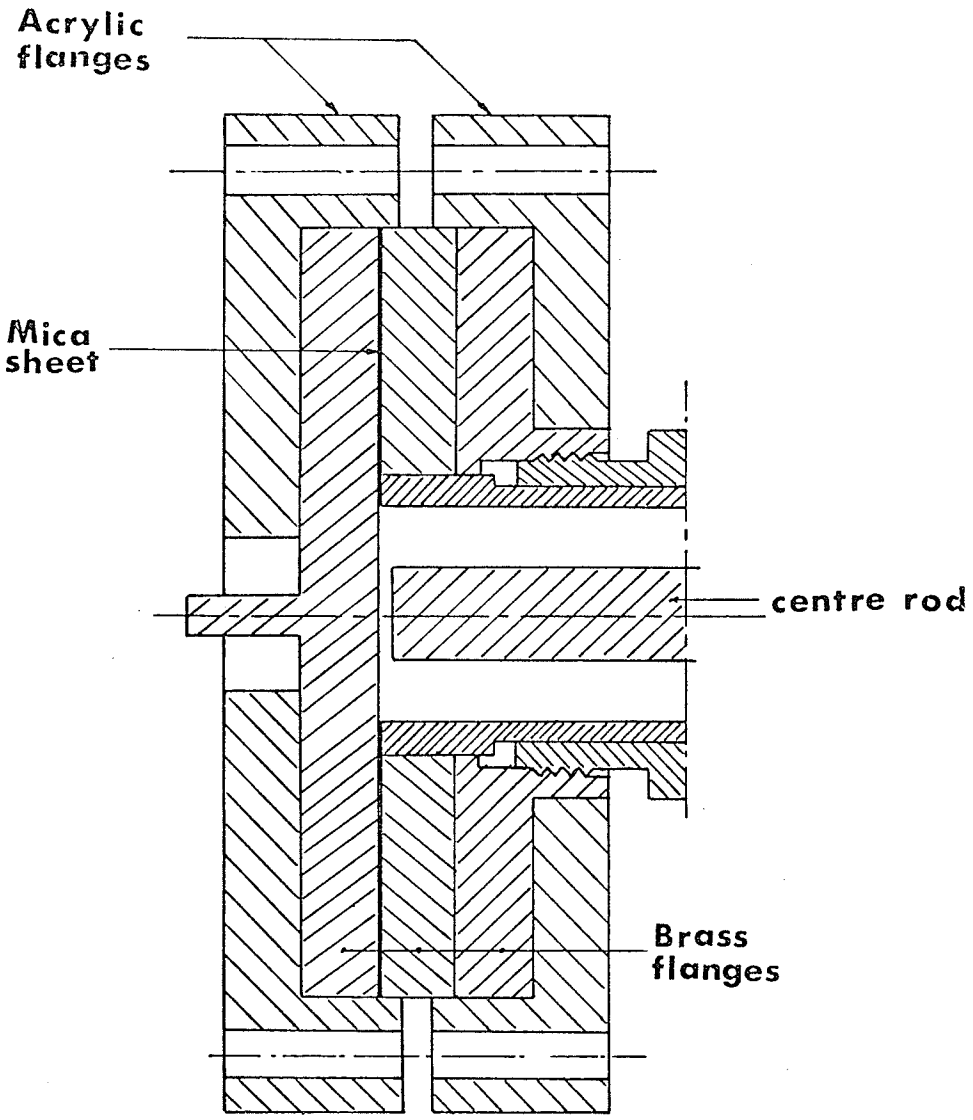

Fig. 4.4. Sample holder.

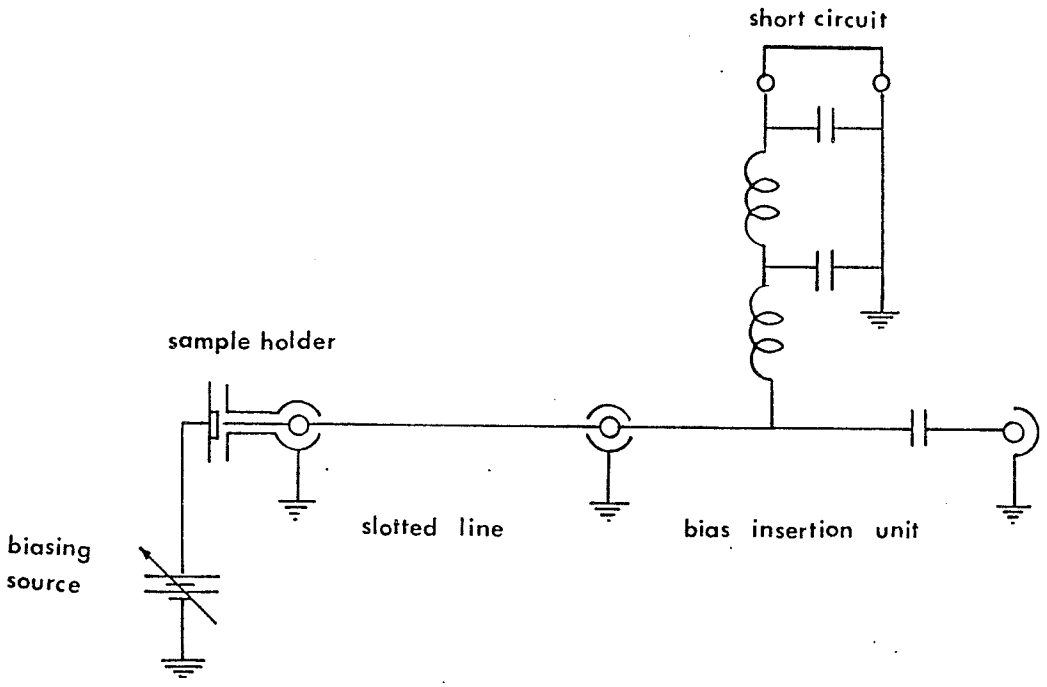

Fig. 4.5. Sample biasing circuit.

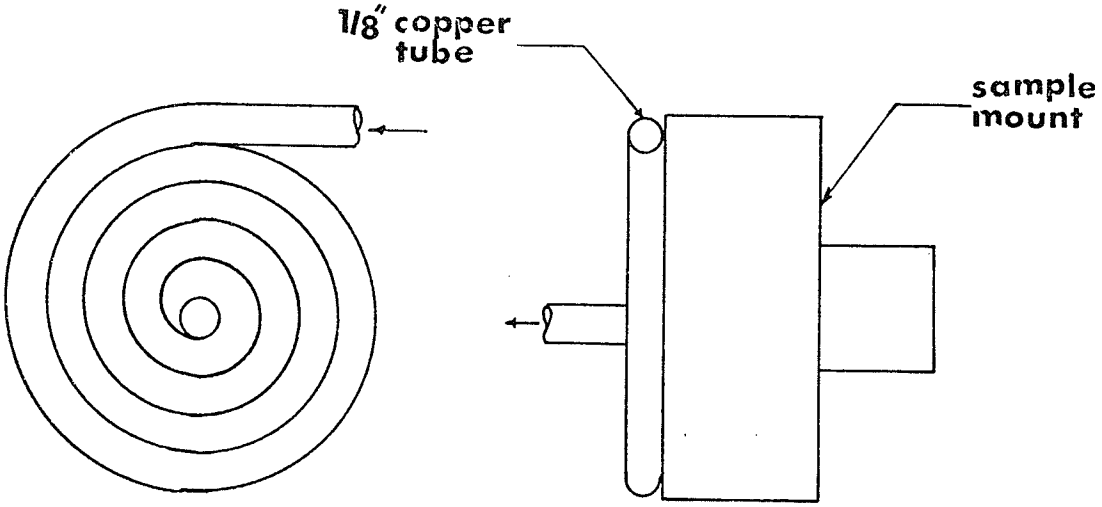

Fig. 4.6. Cooling attachment.

sample holder was replaced by one of longer length and which made a firm contact with the end plate. Positions of standing wave minima were determined by measuring two points on the sides of each minimum 3 dB above its level. This was done for different frequencies over the whole frequency range. The location of the end plate was then determined using the fact that the distance between each minimum and the short circuit end must be equal to integral numbers of half wavelengths. The final value, consistent with the slotted line scale, was -6.475 cm.

3. The short circuit was then removed and the mount containing the sample was connected to the slotted line. Again the position of two points around the minima and 3 dB above its level were recorded. These results were fed to the computer to obtain the complex permittivity at different bias conditions.

4. To measure the effect of temperature on permittivity, the sample mount was heated by a constant flow of hot water for about one hour to allow it to reach a stable temperature condition before any measurements were carried out. The temperature was measured using a copper-constantan thermocouple and special thermocouple potentiometer [Cambridge portable potentiometer No. L-361086].

4.3.3. *Sources of error*

1. Slotted line attenuation errors: In this series of measurements the line attenuation was neglected even though it might introduce certain errors. These errors, however, are negligable since the line attenuation is very small as is seen by the high short-circut VSWR which results.

2. Frequency deviation errors: Frequency deviation affects the

position of minima during measurements. It also affects the receiver reading due to deviations in the i.f. frequency. This error was minimized by allowing the oscillators enough warm-up time and by taking readings at all available minima on the line and averaging them.

3. Leakage capacitance errors: Capacitance C_o was estimated using the actual dimensions of the sample holder capacitor. This is not its time value, due to the leakage capacitance, and a correction was applied using an experimentally derived curve given by Stuchly et al [64].

4.4. *Measurement of I-V Characteristics*

The circuit shown in Fig. 4.7 in conjunction with Tektronix type 549 storage oscilloscope were used to record the current-voltage characteristic of the amorphous semiconductors. The voltage and current were recorded by increasing the voltage slowly up to a certain value and then the voltage was kept constant until the current reached its final value.

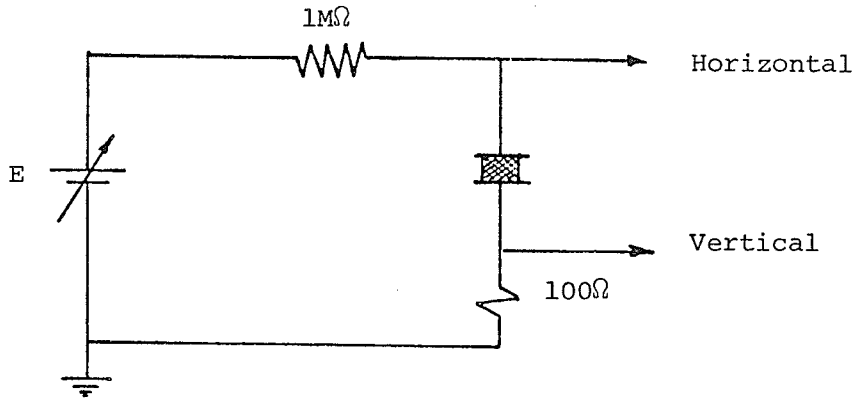

Fig. 4.7. Schematic illustration of the circuit used for measuring the I-V characteristic.

CHAPTER 5

RESULTS AND DISCUSSION

5.1. *Theory of Polarization and Absorption*

The resonance absorption may occur in solids containing dipolar molecules with large moments of inertia due to rotational oscillations of the molecules about their equilibrium positions [18, 19]. Consider a set of oscillating dipolar molecules in which each molecule can be considered as a linear harmonic oscillator having the moment of inertia I, the dipole moment ξ and the corresponding natural frequency $\omega_o/2\pi$. If the concentration of such molecules is assumed to be so small that the interaction between them can be neglected then the equation of vibration of each oscillator at an applied field $\vec{E}$ can be written as

$$\frac{d^2\theta}{dt^2} = -\omega_o^2\theta + \frac{|\vec{\xi} \times \vec{E}|}{I} \qquad (5.1)$$

where θ is the angular displacement.

In the case of polarization of a dielectric by an applied alternating field, a phase shift will occur between the dipole oscillations and the field due to the damping forces. Also, if the field is removed, the dipole will relax to its original state in a time dependent mainly on the collision process within the dielectric. Using the decay factor for the polarization proposed by Frölich [18]

$$\alpha(t) = \alpha(o)e^{-t/\tau}\cos(\omega_o t + \psi) \qquad (5.2)$$

where ψ is the phase angle by which the polarization lags the driving field. The real relative permittivity (dielectric constant) is given by

$$\varepsilon' - \varepsilon_\infty = \frac{\Delta\varepsilon}{2}\left(\frac{1 + \omega_o(\omega + \omega_o)\tau^2}{1 + (\omega + \omega_o)^2\tau^2} + \frac{1 - \omega_o(\omega - \omega_o)\tau^2}{1 + (\omega - \omega_o)^2\tau^2}\right) \tag{5.3}$$

and the imaginary relative permittivity is given by

$$\varepsilon'' = \frac{\Delta\varepsilon}{2}\left(\frac{\omega\tau}{1 + (\omega + \omega_o)^2\tau^2} + \frac{\omega\tau}{1 + (\omega - \omega_o)^2\tau^2}\right) \tag{5.4}$$

where

$$\Delta\varepsilon = \frac{2}{\pi}\int_o^\infty \varepsilon_2(\omega)\,\frac{d\omega}{\omega} \tag{5.5}$$

which can be determined from experimental data with a reasonable accuracy. At constant temperature ε'' as a function of ω has a maximum value when $\omega = \omega_m$. By means of differentiation

$$\frac{\partial\varepsilon''}{\partial\omega} = o \tag{5.6}$$

we can obtain ω_m and it is

$$\omega_m = \frac{1}{\tau}\sqrt{(1 + \omega_o^2\tau^2)} \tag{5.7}$$

and hence the maximum value of ε''

$$\varepsilon''(\omega_m) = \frac{1}{2}\Delta\varepsilon\sqrt{1 + \omega_o^2\tau^2} = \frac{1}{2}\Delta\varepsilon\omega_m\tau \tag{5.8}$$

If $\omega_o\tau >> 1$ we have

$$\omega_m \simeq \omega_o \tag{5.9}$$

and

$$\varepsilon''_{max} = \varepsilon''(\omega_m) \simeq \frac{1}{2}\Delta\varepsilon\,\omega_o\tau \tag{5.10}$$

Thus, the maximum and minimum values of ε' can be determined using the equations

$$\varepsilon'_{max} = \varepsilon_\infty + \frac{\Delta\varepsilon}{2}\omega_o\tau = \varepsilon_\infty + \frac{\varepsilon''_{min}}{2} \tag{5.11}$$

$$\varepsilon'_{min} = C_\infty - \frac{\Delta\varepsilon}{2}\omega_o\tau = \varepsilon_\infty - \frac{\varepsilon''_{min}}{2} \qquad (5.12)$$

The half-value points, where ε'' falls to 1/2 of its maximum value, corresponds to $\pm\Delta\varepsilon = \frac{1}{\tau}$. Thus, the longer the relaxation time τ, the sharper the resonance.

In the following, experimental results will be presented and then followed with discussion based on the theory.

5.2 *Experimental Results of the Amorphous Semiconductor* $Si_{12}Ge_{10}As_{30}Te_{48}$

5.2.1 *Current-voltage characteristics*

Figure 5.1 shows the oscillograms of the current-voltage characteristics of a sample having the dimensions of that described for the coaxial line technique. In each figure we can see the final equilibrium in current-voltage characteristics of the sample under different bias conditions. We are interested only in the final state on each curve because this gives the condition at which the permittivity is measured at a specified bias field. The figure shows also that the material has an ohmic current-voltage characteristic up to a certain threshold voltage, and then the voltage across its drops while the current increases up to certain current and then it follows another ohmic curve with higher conductivity. Hence, the amorphous semiconductor under investigation has two conductivity states. It switches from the low conductivity state to the high one at a certain voltage, which is dependent on temperature and the size of the sample [48].

5.2.2 *Absorption spectrum*

Figure 5.2 shows the real and imaginary parts of the complex

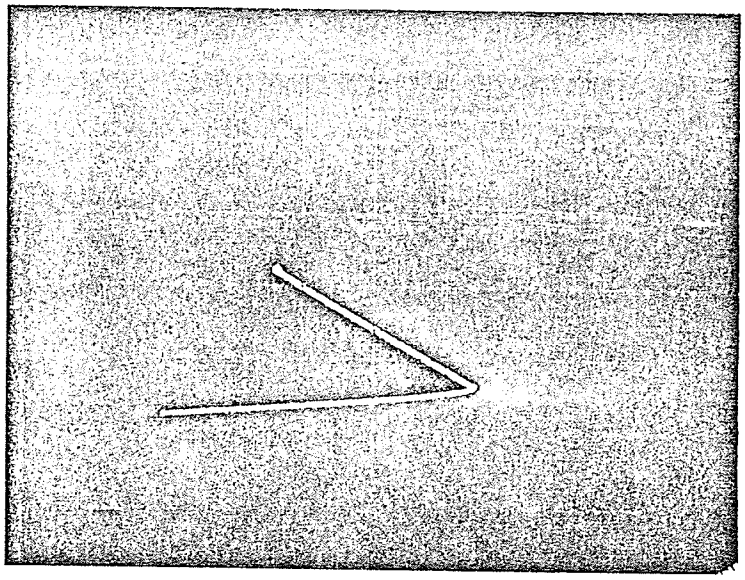

(a)

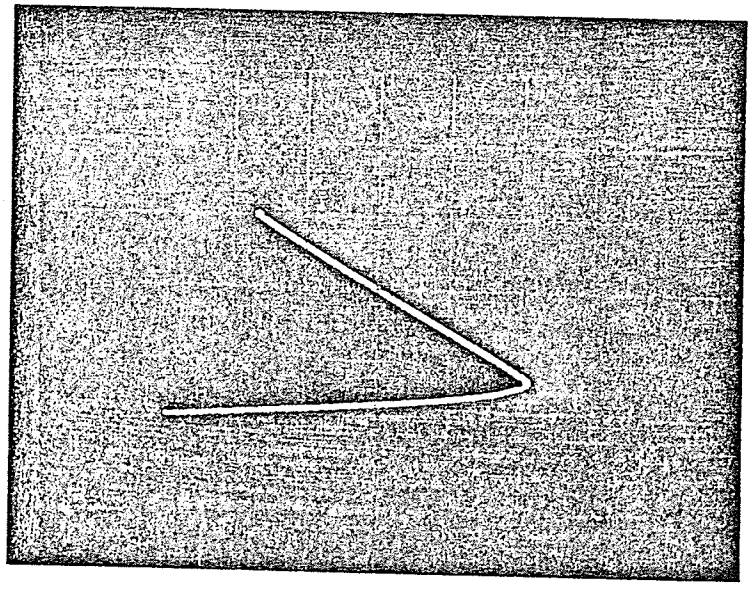

(b)

Fig. 5.1. Current-voltage characteristics of the amorphous semiconductor $Si_{12}Ge_{10}As_{30}Te_{48}$.
Scale: horz. 100V/div.,; vert. 0.2 mA/div.
Voltage: a, 700; b, 800.

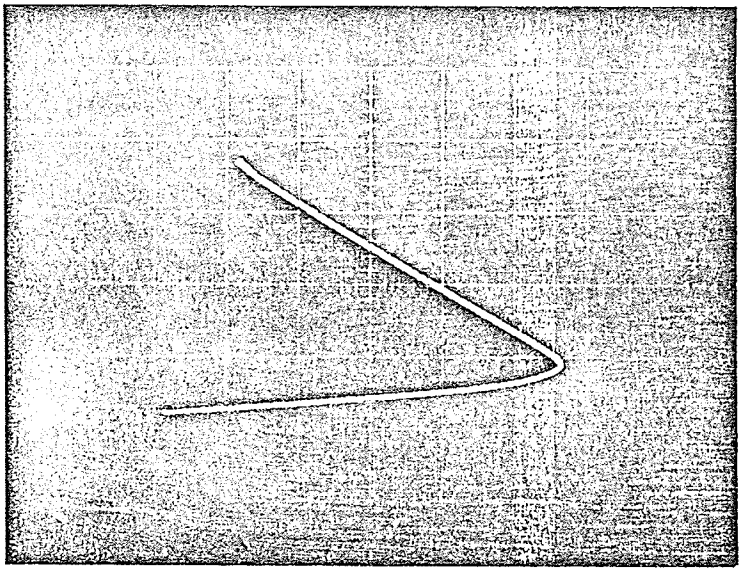

(c)

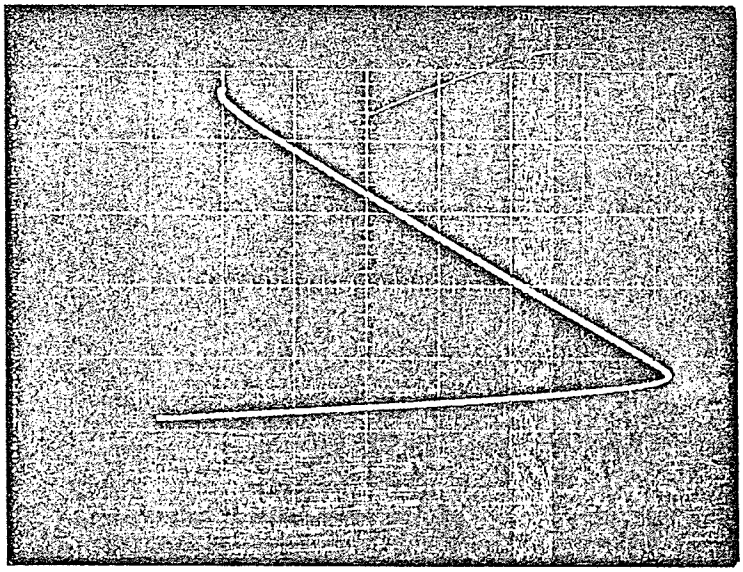

(d)

Fig. 5.1. Current-voltage characteristics of the amorphous semiconductor $Si_{12}\ Ge_{10}\ As_{30}\ Te_{48}$
Scale: horz. 100 V/div.; vert. 0.2 mA/div.
Voltage: c, 900; d, 1000.

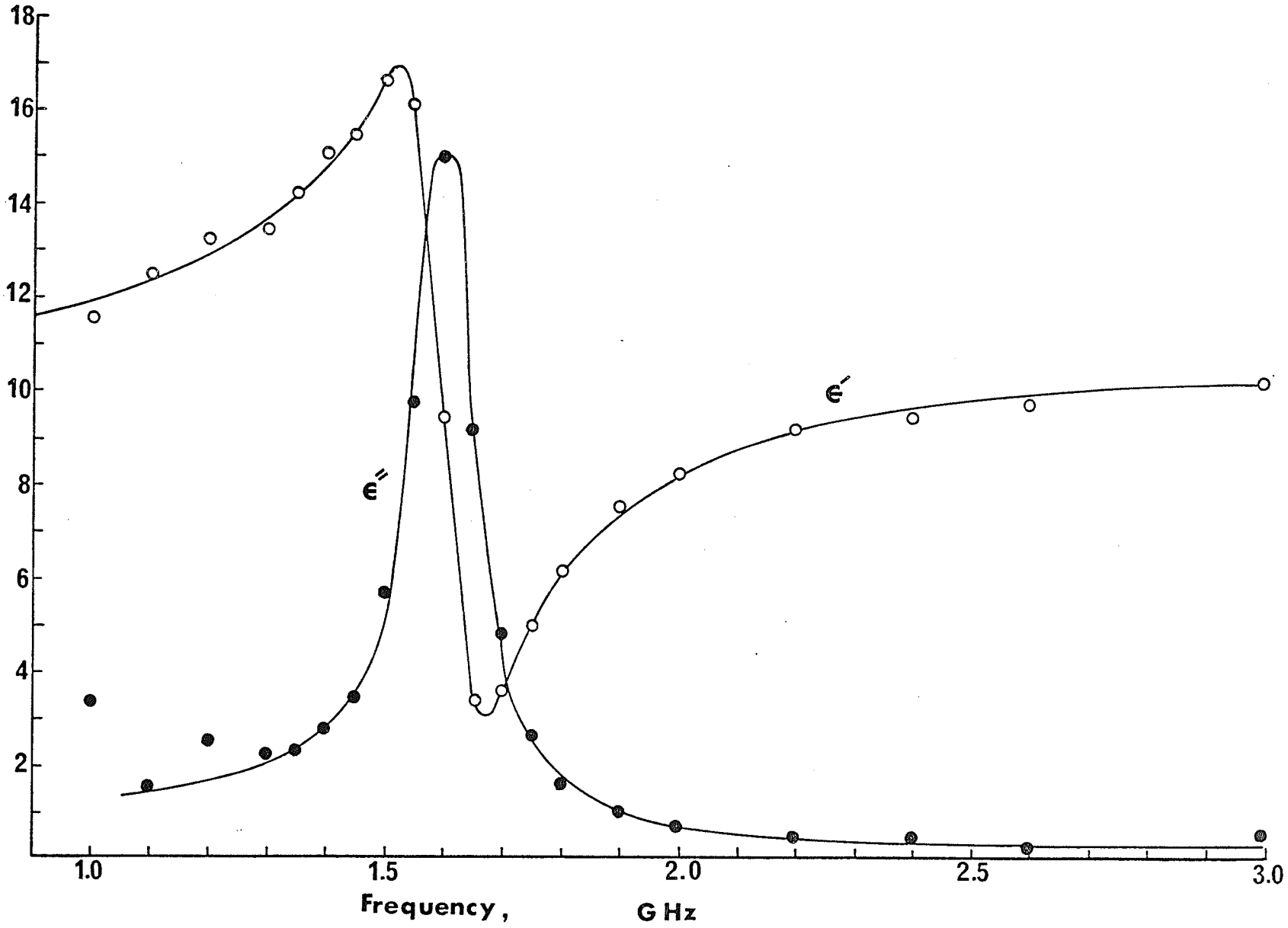

Fig. 5.2. Permittivity of amorphous semiconductor Si_{12} Ge_{10} As_{30} Te_{48} as a function of frequency.

permittivity of the amorphous semiconductor as a function of frequency, in the frequency range 1-3 GHz, it is clear that the material shows a resonance absorption at a resonance frequency of 1.6 GHz.

5.2.3. *The effect of temperature on the absorption spectrum*

The temperature range was limited to 10°C-42°C as a wider range may lead to serious changes in the dimension of the sample mount, which may in turn lead to the separation of the contact surfaces of the sample. This separation will cause serious errors in the permittivity measurements. Figure 5.3 shows the effect of temperature on the absorption spectrum. The resonance frequency increases with increasing temperature.

5.2.4. *Complex permittivity of the amorphous semiconductor in the presence of high d.c. electric field*

The permittivity of the amorphous semiconductor has been measured at a frequency of 4 GHz in the presence of fields up to 20 Kv/cm, and at the frequency 30 GHz in the presence of fields up to 4 Kv/cm. No appreciable change was observed in the real permittivity under these bias fields.

5.3. *Experimental Results of Anthracene Organic Crystals*

5.3.1 Frequency dependence of the relative real permittivity (dielectric constant)

The dielectric constant of anthracene in a direction perpendicular to a-b plane of the crystal, was measured in the frequency range 1 to 4 GHz. The dielectric constant ε_r' was found to be equal to 3.7. Figure 5.4 shows that the dielectric constant of anthracene is in

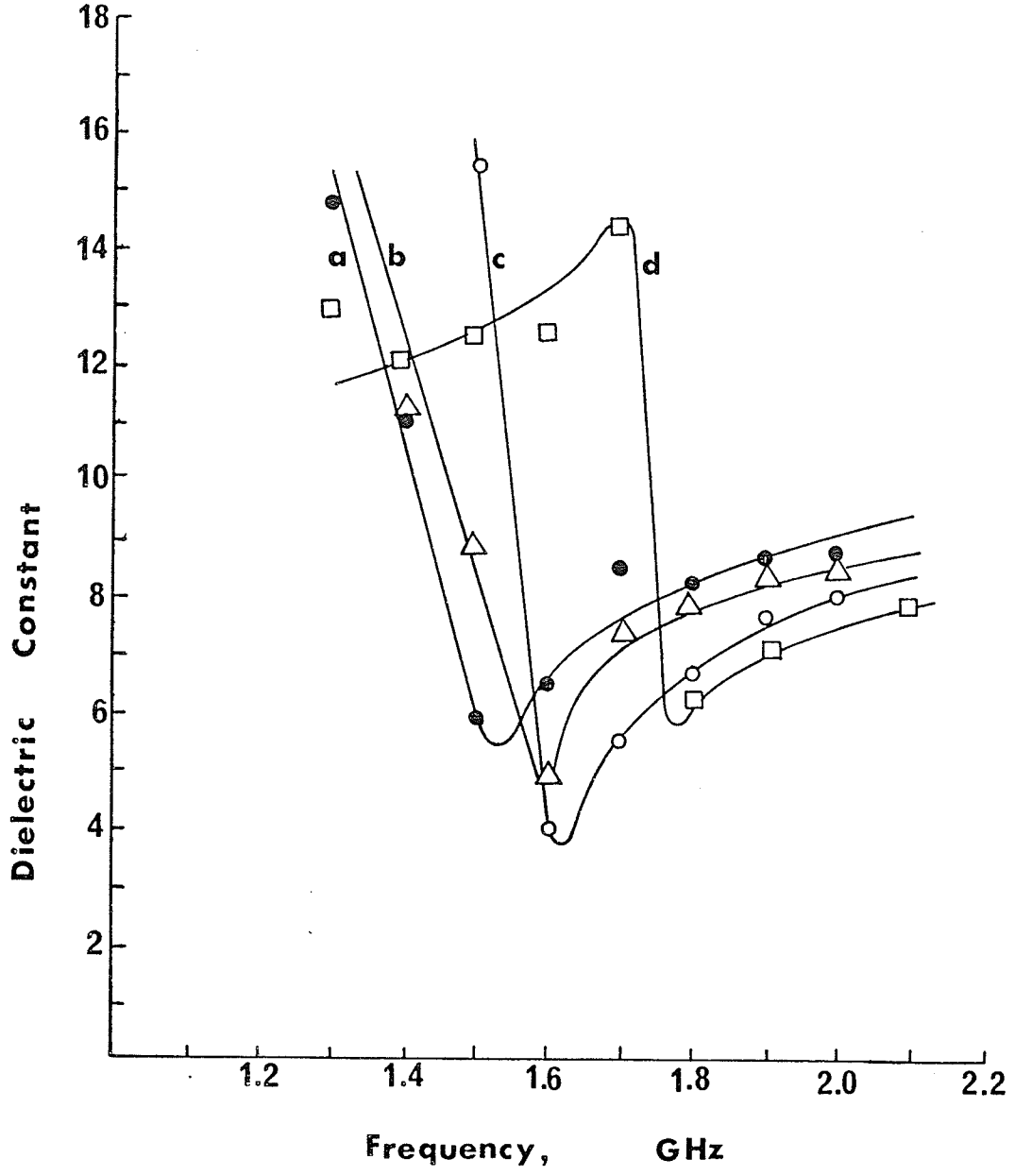

Fig. 5.3. Permittivity of amorphous semiconductor Si_{12} Ge_{10} As_{30} Te_{48} as a function of frequency and termperature. Temperature: a, 13°C; b, 20°C; c, 33°C; d, 42°C.

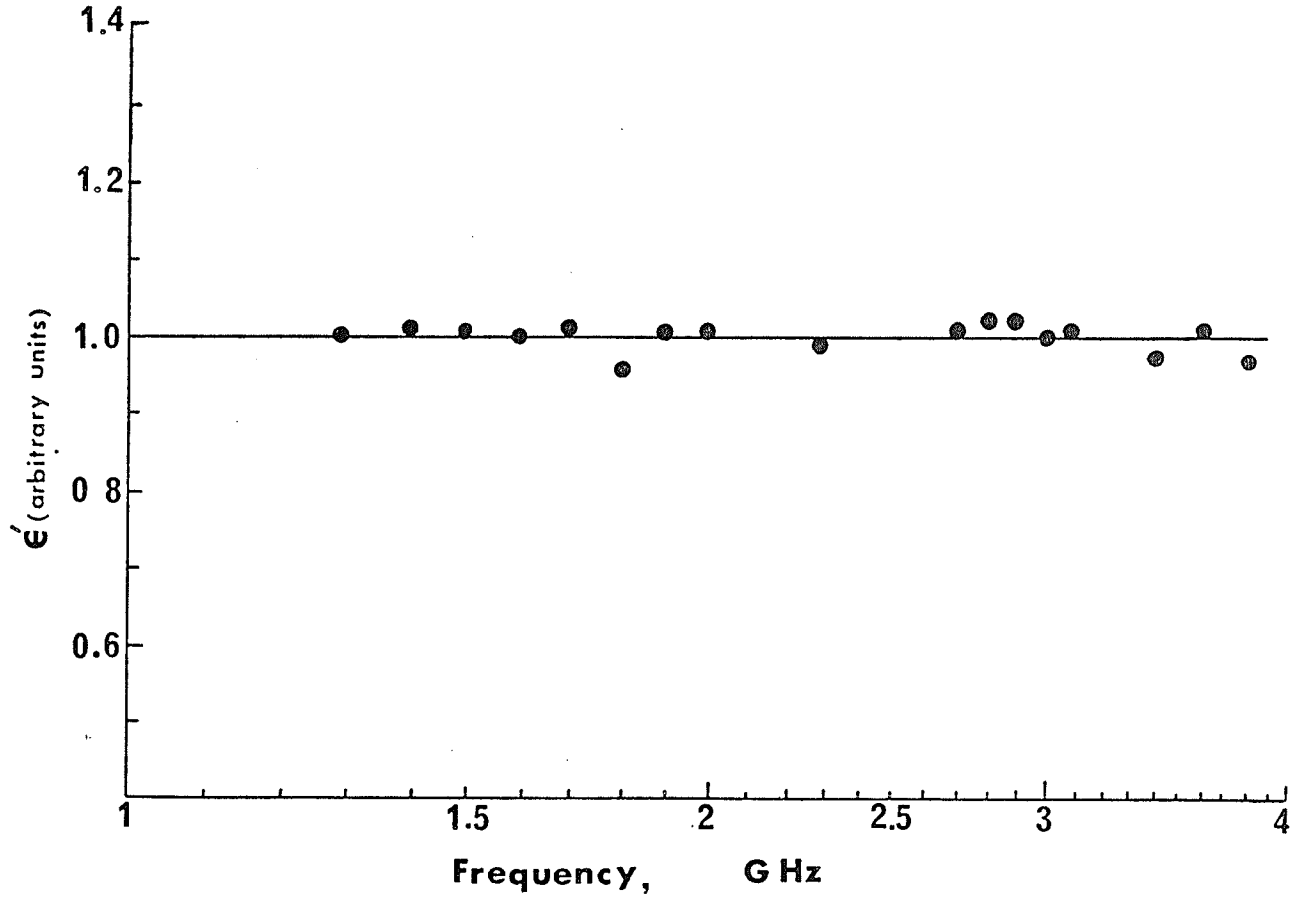

Fig. 5.4. Relative real permittivity of anthracene as a function of frequency.

independent of frequency in the frequency range used.

The dielectric constant in a direction parallel to the a-b crystal plane was also measured to be 2.38 in the frequency range 29-31 GHz.

5.3.2 *Temperature dependence of relative real permittivity*

The relative real permittivity was measured at the frequency 2 GHz over the temperature range 10°C-50°C. The relative real permittivity is not sensitive to temperature, as shown in Fig. 5.5.

5.3.3 *Relative real permittivity of anthracene in the presence of high d.c. field.*

An electric field ranging from 0 to 20 Kv/cm was applied to the anthracene sample perpendicular to the a-b plane of the crystal and parallel to the microwave field, at a frequency of 30 GHz, and a field up to 4 Kv/cm parallel to the a-b plane of the crystal at a frequency of 4 GHz. No change in the dielectric constant was observed under the above conditions.

5.4. *Discussion of Results*

5.4.1 *Amorphous semiconductor* $Si_{12}\ Ge_{10}\ As_{30}\ Te_{48}$

a) Resonance Absorption

Resonance absorption in dielectrics is well known to be due to displacement of charges bound elastically to an equilibrium position [3, 18]. This behaviour has been referred to as optical polarization as its resonance frequency lies in the optical range. The mechanisms responsible for resonance absorption are either electronic or atomic

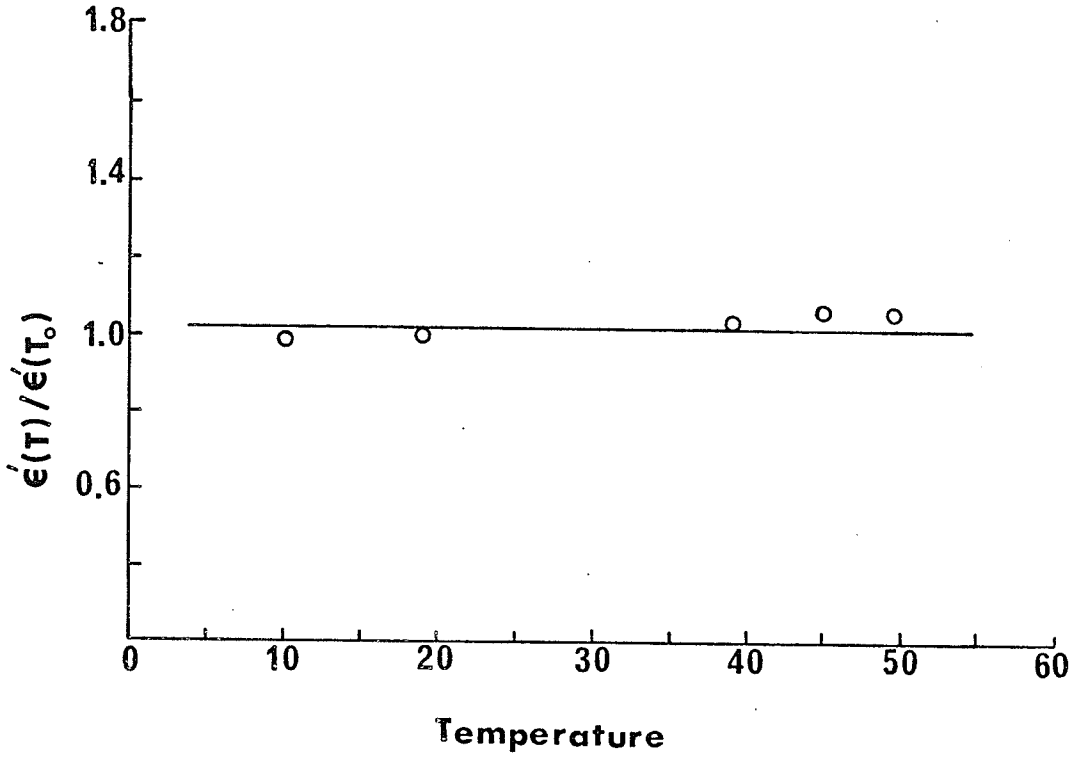

Fig. 5.5. Relative real permittivity of anthracene as a function of temperature at 2 GHz.
(T_o = 23°C).

polarization, and thus the relaxation spectra may lie either in the visual or infrared regions. Frölich [18, 19], however, suggested that the resonance absorption may also be of importance in solids containing dipolar molecules with large moments of inertia. The resonance in this case is due to rotational oscillations of the molecules about their equilibrium positions. The relaxation time of such a behaviour, however, has not yet been investigated.

It is believed that the resonance absorption in amorphous semiconductor $Si_{12}\ Ge_{10}\ As_{30}\ Te_{48}$ observed is due to the rotational vibration of dipolar molecules about their equilibrium position. There are two reasons to support this suggestion. First, the resonance frequency of the absorption spectrum is very low compared to that caused by atomic polarization [18]; and second, the resonance frequency of the absorption spectra caused by atomic or electronic polarization is not very sensitive to temperature, while the one in $Si_{12}\ Ge_{10}\ As_{30}\ Te_{48}$ is fairly sensitive to temperature changes as shown by Fig. 5.3.

From the experimental curves given in Fig. 5.2 and Eq. (5.9), and on the basis of the fact that ε'' falls to 1/2 of its maximum value at a frequency $(\omega - \omega_o) \equiv \frac{1}{\tau}$; the values of $\Delta\varepsilon$ and τ are found to be

$$\Delta\varepsilon \simeq 1.2$$

$$\tau \simeq 2.45 \times 10^{-9} \text{ sec}$$

This relaxation time τ, in terms of the period of oscillation of the dipolar molecules, which is of the order of 0.62×10^{-9} sec., is a relatively short relaxation time. This may imply that the damping force is fairly large, in this material. This damping force may be due to

the high collision rate of the molecules with their surrounding molecules.

In order to compare the experimental results in Fig. 5.2 quantitatively with the theory outlined in Section 5.1, the values of $\Delta\varepsilon$, τ, and f_o obtained from the experimental data are substituted into Eqs. (5.2) and (5.3), which are then solved by the computer. The results are shown in Figs. 5.6 and 5.7. It can be seen that the experimental results are in good agreement with the theory. This leads to the following two conclusions:

i) As the theoretical equations were derived on the basis of classical mechanics and thermodynamics, this indicates that the dipolar molecules responsible for this absorption spectra are large in size and have a fairly large moment of inertia, and,

ii) These theoretical equations were also derived without taking into account the interaction between oscillators. One may therefore deduce that the number of dipolar molecules per unit volume is fairly small, or they are shielded from each other by another neutral medium.

Summarizing the above results, we can state that the observed absorption spectra is due to the rotational vibration of large dipolar molecules with large moment of inertia about their equilibrium position. The interaction between these dipoles is fairly weak, but their collision rate with the surrounding molecules is high, thus giving rise to a short relaxation time.

The formulation of these dipolar molecules and their behaviour may be explained by looking at the structure of amorphous alloy given by Adler et al [2]. They have proposed that the configuration of the amorphous alloy $Ge_{15}\ As_4\ Te_{81}$, is roughly 30% Te atoms with one Te

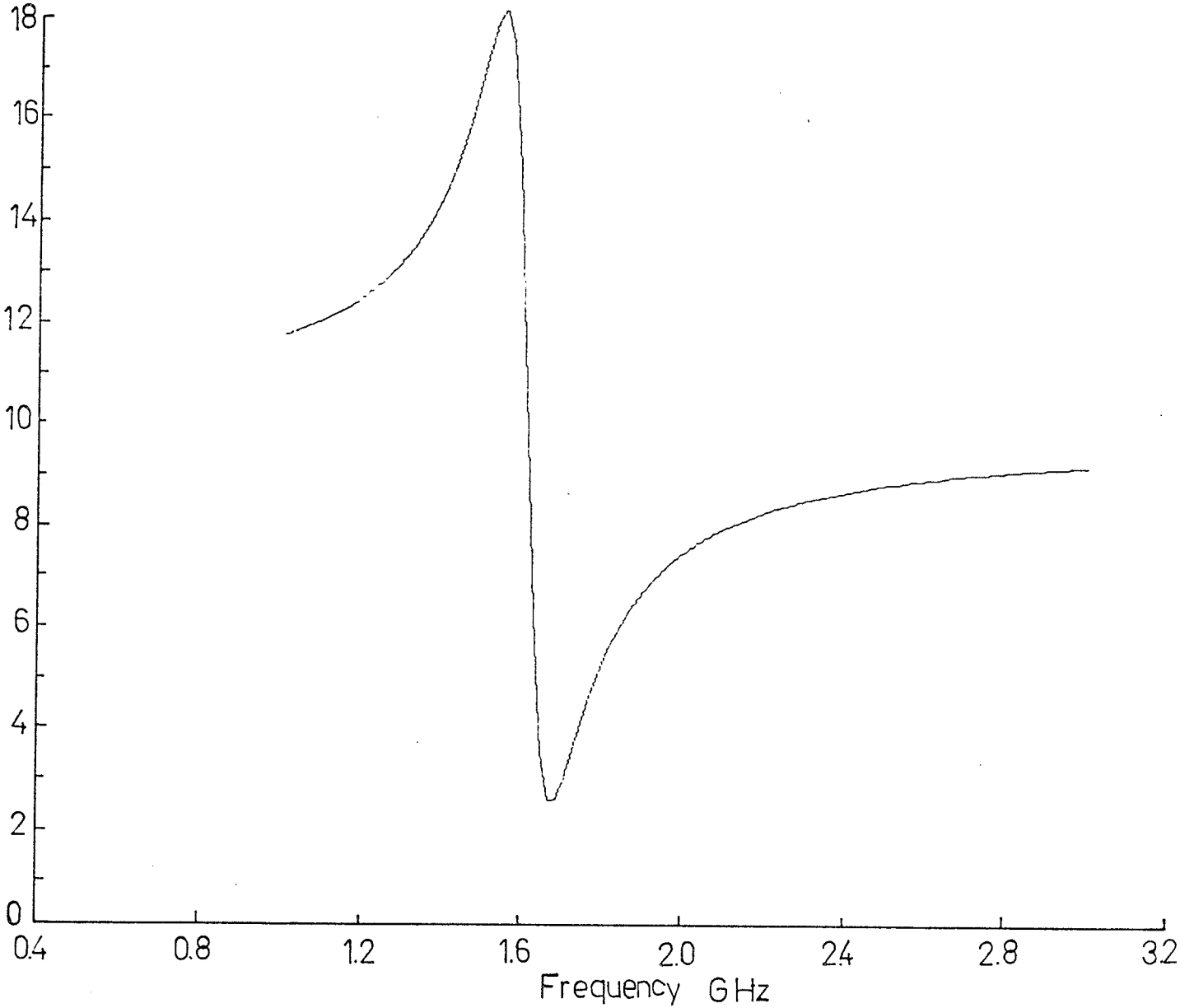

Fig. 5.6. Computed real permittivity of amorphous semiconductor Si_{12} Ge_{10} As_{30} Te_{48} as a function of frequency.

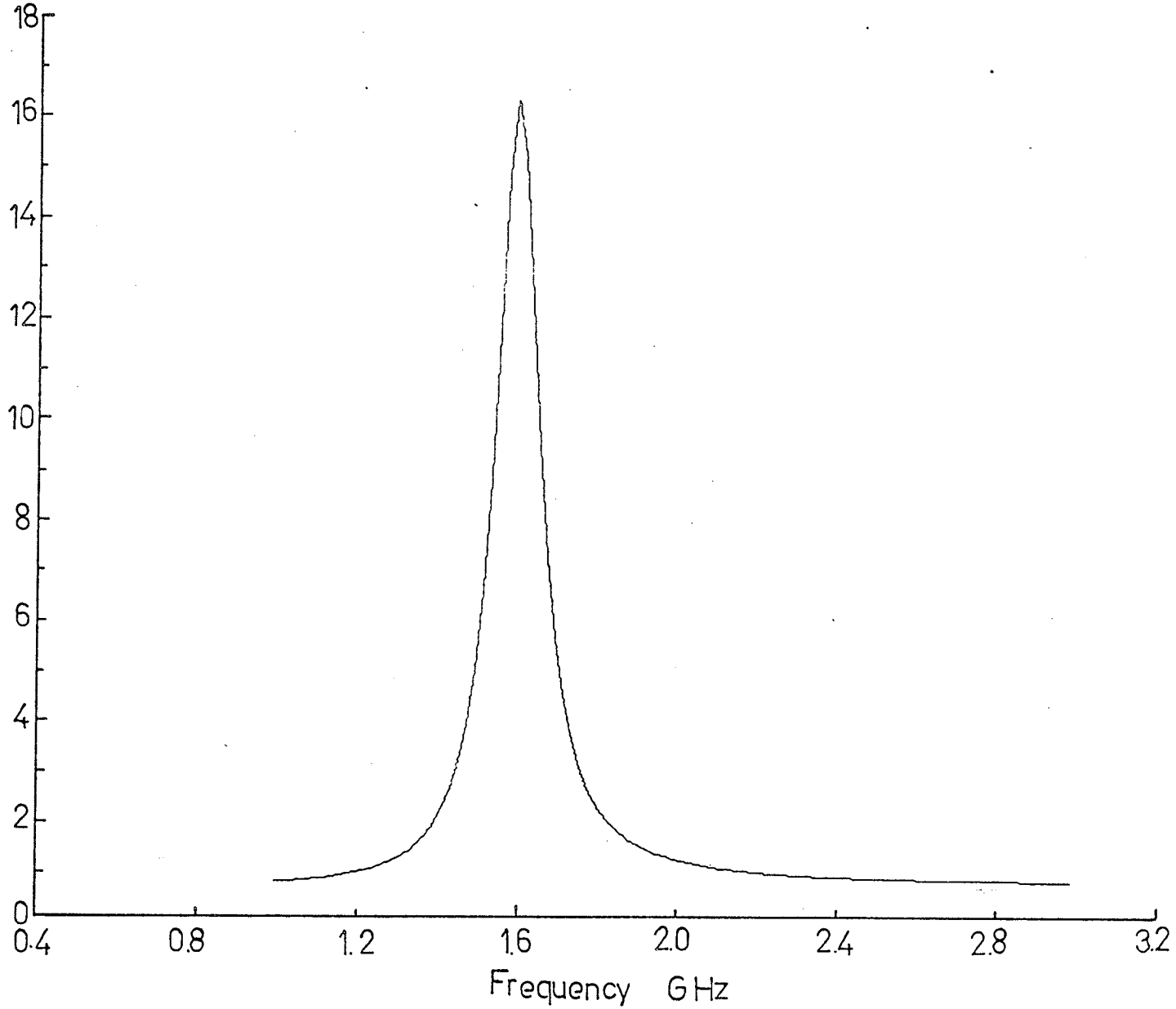

Fig. 5.7. Computed imaginary permittivity of amorphous semiconductor $Si_{12}\ Ge_{10}\ As_{30}\ Te_{48}$ as a function of frequency.

and one Ge neighbour. The remaining Te atoms are at varying though not large distances from the Ge atoms and will have As neighbours, etc. It has also been reported [65a, 48a] that the phase separation occurs, frequently on a fine spatial scale, in many glasses formed by cooling melt solutions. This phase transition has been observed in the amorphous composition $Si_{12.6}\ Ge_{10}\ As_{30}\ Te_{47.4}$ by Phillips et al [48a]. The composition of this material is very close to the amorphous semiconductor under investigation, so it is likely that such a phase transition in these materials may lead to the formation of dipolar molecules of fairly large size. The applied alterating electric field will cause these dipoles to rotationally vibrate. Also these dipoles are separated from each other by the phases of the rest of the composition, so the interaction between them is relatively weak.

The increase of the resonance frequency of the absorption spectra with increasing temperature can be explained as follows: Referring to Eq. (5.1) the increase in ω_o can be due either to a decrease in the moment of inertia of the dipole or to an increase in the binding forces between it and its surroundings. The latter reason is more reasonable, as any change in the moment of inertia will not be of appreciable effect in this small temperature change. The binding forces depends on the internal fields, so the observed behaviour of the resonance frequency suggests that these forces increase with increasing temperature. This can be explained qualitatively, as these dipoles are "frozen in" in the material so the increase in energy by increasing temperature will increase their potential energy and hence their natural frequency ω_o as the potential energy of each dipole is equal to $1/2\ I\ \omega_o^2$.

b) Complex permittivity in the presence of high d.c. electric

field.

The experimental results show that the dielectric constant of the amorphous semiconductor $Si_{12}\ Ge_{10}\ As_{30}\ Te_{48}$ does not change with the presence of high electric field. At this low conductivity state the main carriers contributing to conductivity are hopping electrons [45a]. It would be expected (see Eq. (2.14)), that when the material is in the low conducitivity state the carriers contributing to the dielectric constant at high fields up to the threshold field are negligible. Although in the high conductivity state the increase in conductivity can be as high as 10^5, the transition between the two states occurs only in one or more filaments of size (of the order of a few microns) much smaller than the electrode size. Their formation is mainly due to diffusion of certain atoms towards the region to make the structure of the filamentry path more crystalline, but not cause much increase in carriers. The impedance of the sample at the high conductivity state may then be represented by the equivalent circuit shown in Fig. 5.8, in which C_1 and G_1 are the capacitance and conductance of the conductive filament. Since the filament cross section area is very small compared to the sample surface area, C_1 is very small irrespective of the magnitude of the change in the real permittivity of the conductive channel. Referring to Fig. 5.1, maximum G_1 obtained during measurements was 10^{-5} mho which is small compared with the loss capacitance $\varepsilon_r'' C_o$ which is larger than 10^{-3} mho. Hence, the contribution of G_1 to the absorption in the sample is very small. This is why the transition from the low conductivity to the high conductivity state does not affect the complex permittivity of the sample.

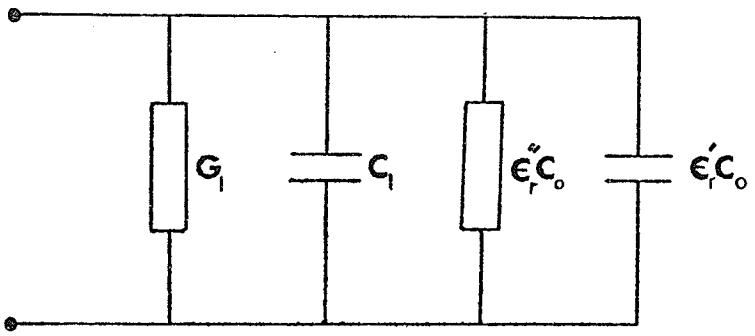

Fig. 5.8. Equivalent circuit for amorphous semiconductor $Si_{12}\ Ge_{10}\ As_{30}\ Te_{48}$ sample in the high conductivity state.

Table 1

Dielectric constant of Anthracene Crystals

	10^{-4}-10^{3} Hz [31]	5.07 x 10^{10} Hz [17]	4.6 x 10^{14} - 7.4 x 10^{14} Hz [2a]
ε_{11}	2.51	2.35	---
ε_{22}	2.99	2.70	2.76
ε_{33}	4.11	3.70	3.93

5.4.2 *Anthracene organic crystals*

a) Frequency dependence of the relative real permittivity (dielectric constant).

The dielectric constant of anthracene has been measured at various frequencies and orientations [2a, 17, 31] and the results are summarized in Table 1. where ε_{11}, ε_{22}, and ε_{33} are the dielectric constant in directions corresponds to the a, b and c crystal directions. It should be noted that the value of the dielectric constant, 3.7, was measured in the frequency range 1-4 GHz and in the direction C', which is perpendicular to the a-b crystal plane, and the value 2.38 in the frequency range 29-31 GHz and in the direction parallel to the a-b plane. So the value 2.38 is expected to be an average value of the dielectric constant in the directions a and b. Comparison of these results with the results in Table 1, indicates that the real permittivity of anthracene is constant over all these frequency ranges.

From the above results it is likely that the mechanism responsible for polarization in anthracene is electronic polarization. As this type of polarization does not experience changes over the frequency

ranges aforementioned . Since the electronic polarization is temperature independent [18] the dielectric constant of anthracene would be expected to be temperature independent as shown in Fig. 5.5.

b) Dielectric constant of anthracene in the presence of high d.c. electric fields

The experimental results show that there is no appreciable change in the dielectric constant of anthracene in the presence of high d.c. electric fields up to 20 Kv/cm. Hwang et al [29] have reported that at room temperature the anthracene has a low conductivity of the order 10^{-13} mho cm^{-1} for fields up to about 30 Kv/cm. The low conductivity indicates that the concentration of carriers is very small and hence their contribution to the dielectric constant in the presence of high electric field is negligible.

CHAPTER 6

CONCLUSIONS

On the basis of the results and discussion given in Chapter 5, the following conclusions are drawn.

I. Amorphous semiconductor $Si_{12}\ Ge_{10}\ As_{30}\ Te_{48}$

a) Amorphous semiconductor $Si_{12}\ Ge_{10}\ As_{30}\ Te_{48}$ shows a resonance absorption in the frequency range 1-4 GHz. The resonance appears at the frequency of 1.6 GHz corresponding to a relaxation time of 2.45×10^{-9} sec, at room temperature (293°K).

b) The resonance frequency of the absorption spectrum increases with the increasing temperature in the temperature range 13-42°C.

c) The dielectric constant of the amorphous semiconductor $Si_{12}\ Ge_{10}\ As_{30}\ Te_{48}$, at room temperature, is not sensitive to bias fields up to 20 Kv/cm at the frequency 4 GHz, and up to 3 Kv/cm at the frequency 30 GHz.

d) The resonance absorption is attributed to rotational vibration of dipolar molecules having large moments of inertia about their equilibrium positions. The experimental results are in close agreement with the theoretical equations based on this model. The increase of the resonance frequency with increasing temperature is attributed to an increase in the potential energy of the dipolar molecule due to an increase in the internal fields as the temperature is increased.

e) The dielectric constant is not affected by high d.c. bias field, and this is due to that the size of the conductive filament being very small compared with the size of the sample.

II. Anthracene Crystals

a) The dielectric constant of anthracene organic crystals is equal to 3.7 in a direction perpendicular to the a-b crystal plan in the frequency range 1-4 GHz, and 2.38 in a direction parallel to the a-b crystal plane in the frequency range 29-31 GHz.

b) The dielectric constant is not sensitive to temperature changes from 10°C to 50°C in the frequency range 1-4 GHz.

c) The dielectric constant is not sensitive to d.c. bias fields up to 20 Kv/cm at the frequency of 4 GHz, and up to 3 Kv/cm at the frequency of 30 GHz.

d) The mechanism responsible for the above phenomena in anthracene may be electronic polarization and this explains why the dielectric constant is not sensitive to temperature.

e) The dielectric constant is not affected by the applied d.c. bias field because the carrier concentration is too small to show the effect.

REFERENCES

1. Abaulina-Zavaritskaya, E.I., "Electrical properties of germanium at very low temperatures", Soviet Phys. JETP (English transl.), 3, 984-985 (1957).

2. Adler, D., Cohen, M., Fagen, E., and Thompson, J., "Valence electron configuration of Te in Amorphous TeGe alloys", J. Non-Crystalline Solids, 3, 204-6 (1970).

2a. Amberger, R.W., and Flammersfeld, A., "Dispersionskurven für Anthrazen, Tetracen, Para-Terphenyle, trans-Stiben und Plastikszintillator NE102A", Z. Naturf., 23a, 311-314 (1968).

3. Anderson, J.C., "Dielectrics", Chapman and Hall Ltd., London, (1963).

4. Arther, J.B., Gibson, A.F., Granville, J.W., "The effect of high electric field on the absorption of germanium at microwave frequencies", Intern. J. Electronics, 2, 145-53 (1956).

5. Bandler, J.W., "Precision microwave measurement of the internal parasitics of tunnel-diodes", IEEE Trans. ED., 15, 275-282 (1968).

6. Barlow, H.M., and Cullen, A.L., "Microwave measurements", Constable (1950).

7. Budd, H.F., "Hot carriers and the path variable method", J. Phys. Soc. Japan, 21, 420-3 (1966).

8. Champlin, K.S., and Armstrong, D.B., "Explicit forms for the conductivity and permittivity of bulk semiconductors in waveguides", Proc. IEEE, 50, 232 (1962).

9. Champlin, K.S., and Krongard, R.R., "The measurement of conductivity and permittivity of semiconductor spheres by an extension of cavity perturbation technique", IRE Trans. MTT, 9, 545-51 (1961).

10. Chapman, S., and Cowling, T.G., "Mathematical theory of non-uniform gases", Cambridge Univ. Press, London and New York (1939).

11. Collin, R.E., "Field theory of Guided waves", McGraw-Hill New York (1960).

12. Conwell, E.M., "High field transport in semiconductors", Solid State Physics, supplement 9, Academic Press (1967).

13. Conwell, E.M., and Vassell, M.O., "High field transport in N-type GaAs", Phys. Rev., 166, 797-821 (1968).

14. Davydov, B., "Velocity distribution of electrons in a gas under the action of an electric field", Phys. Zeib. d. Sowjetunion, 8, 59-70 (1935).

15. Davydov, B., "Velocity distribution of electrons in an electric field. Part II", Phys. Zeils. d. Sowjetunion, 9, 433-48 (1936).

16. Debye, P., "Polar Molecules", Dover Publication, New York (1929).

17. Dix, G., Helberg, H.W., and Wartenberg, B., "Mikrowellenapparatur zur Messung anisotroper Dielektrizitätskonstanten-Beispiel: Anthrazen", Phys. Stat. Sol. (a), 5, 633-36 (1971).

18. Fröhlich, H., "Theory of Dielectrics", Oxford Univ. Press (1958).

19. Fröhlich, H., "Shape of collision-broadened spectral lines", Nature, 157, 478 (1946).

20. Ginzton, "Microwave measurements" McGraw-Hill (1957).

21. Gibson, A.F., Granville, J.W., and Paige, E.G.S., "A study of energy loss processes in germanium at high electric fields using microwave techniques", J. Phys. Chem. Solids, 19, 198-217 (1961).

22. Glover, G.H., "High-field microwave permittivity of electrons in bulk GaAs", J. Appl. Phys., 42, 5590-5 (1971).

23. Guha, S., and Nag, B.R., "Microwave conduction in n-type germanium under hot electron conditions", Proc. Phys. Soc., 90, 427-34 (1967).

24. Gunn, M.W., "Hot electron effect in n-type germanium at 9.392 GC/sec", J. Electronics and Control, 16, 481-91 (1964).

25. Gunn, M.W., and Brown, J., "Measurement of semiconductor properties in a slotted waveguide structure", Proc. IEE, 112, 463-8 (1965).

26. Gutmann, F., and Lyons, L., "Organic semiconductors", John Wiley and Sons, (1967).

27. Hamaguchi and Inuishi, Y., "Conductivity anisotropy of hot electrons in n-type silicon heated by microwave fields", J. Phys. Chem. Solids, 27, 1511-18 (1966).

28. Hasegaw, A., Yamashita, J., "Density matrix approach to a simple hot electron problem", Phys. Chem. Solids, 23, 875-80 (1962).

29. Hwang, W., and Kao, K.C. "Electroluminescence in anthracene crystals caused by field-induced minority carriers at moderate temperatures", J. Chem. Phys., 58. 3511-12 (1973).

30. Iskandar, M.F., and Stuchly, S.S., "A time-domain technique for measurement of the dielectric properties of biological substances", IEEE Trans. IM., 21, 425-29 (1972).

31. Karl, N., Rohrbacher, H., and Siebert, D., "Dielectric tensor and relaxation of photoexcited charge carreres in single crystal anthracene in an alternating field without direct contacts", Phys. Stat Sol.(a), 4, 105-108 (1971).

32. Koenig, S.H., and Gunther-Mohr, G.R., "The low temperature electrical conductivity of n-type germanium", Phys. Chem. Solids, 2, 268-83 (1957).

33. Kohn, W., and Luttinger, J.M., "Quantum theory of electrical transport phenomena", Phys. Rev., 108, 590-611 (1957).

34. Köpetz, H., and Pötzl, H.W., "Microwave conductivity of polar semiconductivity of polar semiconductors in the presence of a high electric field", Electronic Letters, 4, 79-86 (1968).

35. Kurosawa, T., "Notes on the theory of Hot electrons in semiconductors", J. Phys. Soc. Japan, 20 937-42 (1965).

36. Kurosawa, T., "Monte Carlo calculation of hot electron problems", J. Phys. Soc. Japan, 21, 424-26 (1966).

37. Lance, A.L., "Introduction to microwave theory and measurements", McGraw-Hill, New York (1964).

38. Law, H.C., and Kao, K.C., "New approach to the solution of the time-dependent Boltzmann transport equation", Phys. Rev. Letters, 29, 625-28 (1972).

39. Marcuvitz, N., "Waveguide handbook", McGraw-Hill, New York (1951).

40. Mead, C.A., "Transport of Hot electrons in the gold films", Phys. Rev. Letters, 8, 56-57 (1962).

41. Montgomery, C.G., "Technique of microwave measurement", McGraw-Hill, New York (1947).

42. Nag, B.R., and Das, P., "Microwave conducitivity of semiconductors in the presence of high steady electric fields", Phys. Rev., 132, 2514-520 (1963).

43. Nag, B.R., Roy, S.K., and Chatterji, C.K., "Microwave measurement of conducitivity and dielectric constant of semiconductors" Proc. IEEE, 51, 962 (1963).

44. Nathan, M.I., "Anisotroby of the conductivity of n-type germanium at high electric fields", Phys. Rev., 130, 2201-6 (1963).

45. Oliver, D.J., "Electrical properties of n-type gallium arsenide", Phys., Rev., 127, 1045-52 (1962).

45a. Owen, A.E., "Band or hopping conduction in chalcogenide Glasses", J. Non-crystalline Solids, 4, 78-9 (1970).

46. Owen, R.P., "Technique for the measurement of standing-wave ratio at low power level", Proc. IEE, 116, 933-40 (1969).

47. Pearson, A.D., "Memory and switching in semiconducting glasses", J. Non-Crystalline Solids", 2, 1-15 (1970).

48. Petrillo, G.A., "Electronic properties of amorphous semiconductors", M.Sc. Thesis, E.E. Dept. Univ. of Manitoba, (1973).

48a. Phillips, S.V., Booth, R.E. and McMillan, P.W., "Structural changes related to electrical properties of bulk chlcogenide Glasses", J. Non-Crystalline Solids, 4, 510-17 (1970).

49. Price, P.J., "On the theory of Strong field conduction", Phys. Chem. Solids, 8, 136-37 (1959).

50. Prior, A.C., "Avalanch multiplaction and electron mobility in indium animoxide at high electric fields", J. Electronics and control, 4, 165-69 (1958).

51. Reik, H.G., and Risken, H., "Distribution function for hot electrons in many-valley semiconductors", Phys. Rev., 124, 777-84 (1961).

52. Roberts, S., and VonHippel, A., "A new method for measuring dielectric constant and loss in the range of centimeter waves", J. Appl. Phys., 17, 610-16 (1946).

53. Ryder, E.J., "Mobility of holes and electrons in high electric fields", Phys. Rev., 90, 766-69 (1953).

54. Ryder, E.J., Ross, I.M., and Kleinman, D.A., "Electron multiplication in germanium at low temperature", Phys. Rev., 95, 1342-43 (1954).

55. Sclar, N., and Burstein, E., "Impace ionization of impurities in germanium", Phys. Chem. Solids, 2, 1-23 (1957).

56. Shmidt-Tiedmann, K.J., "Tensor theory of the conductivity of warm electrons in cubic semiconductors", Philips Res. Rept., 18, 338-60 (1963).

57. Shokley, W., "Hot electrons in germanium and ohm's Law", Bell System Tech. J., 30, 990-1034 (1951).

58. Smith, R.W., "Current saturation in Piezoelectric Semiconductors", Phys. Rev. Letters, 9, 87-90 (1962).

59. Spitzer, W.G., Cowell, C.R., and Atalla, M.M., "Mean free path of photoexited electron in An", Phys. Rev. Letters, 8, 57-58 (1972).

60. Spratt, J.P., Schwartz, R.F., Kane, W.M., "Hot electrons in metal films: injection and collection", Phys. Rev. Letters, 6, 341-42 (1961).

61. Steele, M.C., and Glickman, M., "High electric field effects in N-Indium antimonide", Phys. Rev., 110, 1204-05 (1958).

62. Stocker, H.J., Barlow, C.A., and Weirauch, D.F., "Mechanism of threshold switching in semiconducting glasses", J. Non-Crystalline Solids, 4, 523-35 (1970).

63. Straton, R., "The influence of interelectronic collisions on conduction and breakdown in covalent semiconductors", Proc. R. Soc. [A], 242, 355 (1957).

64. Stuchly, S.S., Rzepecka, M.A., and Iskander, M.F., "Permittivity measurements at microwave frequencies using Lumped elements", IEEE

Trans. IM, 23, 56-62 (1974).

64a. Sucher, M., and Fox, J., "Handbook of microwave measurements", John Wiley and Sons, New York (1963).

65. Tateno, H., and Kataoka, S.,"Measurements of conductivity and permittivity of semiconductors at microwave frequencies", Bul. Electrotech. Lab., 31, (1966).

65a. Turnbull, D., and Polk, D.E., "Structure of amorphous semiconductors", J. Non-Crystalline Solids, 8, 19-35 (1952).

66. Waiser, W., and Wheatly, "Hot electrons and carrier multiplication in silicon at low temperature", Phys. Rev. Letters, 3, 334-36 (1959).

67. Westphal, W.B., "Dielectric Materials and applications", edited by Von Hippel, A., MIT Press (1966).

68. Wu, S.M., Bridges, E., and Kao, K.C., "Microwave complex permittivities of Si and GaAs semiconductors in the presence of high steady electric fields", Int. J. Electronics, 31, 233-41 (1971).

69. Yamashita, J., and Inoue, K., "Hot electrons in n-type germanium", J. Phys. Chem. Solids, 12, 1-12 (1960).

70. Yokamota, and Brenner, "Organic semiconductors", Chapman and Hall Ltd., London (1964).

71. Zucker, J., V.J. Fowler, and Conwell, E.N., "High-field conductivity in germanium and silicon at microwave frequencies", J. Appl. Phys. (U.S.A.), 32, 2606-11 (1961).